Fault plane modelling of the 2003 August 14 Lefkada Island (Greece) earthquake based on the analysis of ENVISAT SAR interferograms

M. Ilieva, Pierre Briole, Athanassios Ganas, D. Dimitrov, Panagiotis Elias, A. Mouratidis, R. Charara

Fault plane modelling of the 2003 August 14 Lefkada Island (Greece) earthquake based on the analysis of ENVISAT SAR interferograms

M. Ilieva,[a,b] P. Briole,[c,*] A. Ganas,[d] D. Dimitrov,[a] P. Elias[e], A. Mouratidis[f], R. Charara[c]

a. Bulgarian Academy of Sciences, National Institute of Geophysics, Geodesy and Geography, Department of Geodesy, Acad. G. Bonchev str, bl. 3, 1113 Sofia, Bulgaria
b. University of Architecture, Civil Engineering and Geodesy, Faculty of Geodesy, Department of Geodesy and Geoinformatics, 1, Hristo Smirnenski Blvd., 1046 Sofia, Bulgaria
c. Ecole Normale Supérieure, PSL Research University, Laboratoire de Géologie - UMR CNRS 8538, 24 Rue Lhomond, 75005 Paris, France
d. National Observatory of Athens, Institute of Geodynamics, Lofos Nymfon, Thission, 11810 Athens, Greece
e. National Observatory of Athens, Institute of Astronomy, Astrophysics, Space Applications and Remote Sensing, Vas. Pavlou & I. Metaxa, GR-15 236 Penteli, Greece
f. Aristotle University of Thessaloniki, School of Geology, Department of Physical and Environmental Geography, 54124 Thessaloniki, Greece

* Corresponding author.
E-mail addresses: m_b_ilieva@abv.bg (M. Ilieva), pierre.briole@ens.fr (P. Briole), clgdimi@bas.bg (D. Dimitrov), aganas@noa.gr (A. Ganas), pelias@noa.gr (P. Elias), amourati@auth.gr (A. Mouratidis), rana_charara@trimble.com (R. Charara)

Abstract

On 2003 August 14, a M_w = 6.2 earthquake occurred offshore the Lefkada Island in the eastern Ionian Sea, one of the most seismically active areas in Europe. The earthquake caused extended damages in the island, and a number of ground failures, especially along the north-western coast. Seven ascending ENVISAT/ASAR images are used to process six co-seismic interferograms. The ROI-PAC package is used for interferogram generation with the SRTM DEM applied in a two-pass method. The formation of the co-seismic pairs is limited due to the existence of one pre-seismic image only. Dense vegetation is covering the island, which is an obstacle in getting good coherence, since C-band images are used. Nevertheless, ground deformation, of more than 56 mm (two fringes) in the line of sight of the satellite, is detected in all six co-seismic interferograms. By inversion of the data from the observed fringes, a best fitting model of the activated fault is calculated assuming a dislocation in an elastic half space. The inferred fault is a pure dextral strike-slip fault, dipping 59 ± 5 ° eastward, 16 ± 2 km long and 10 ± 2 km wide. It is located north of the fault of the M_w = 6.5 2015 November 17 earthquake, and a 10-15 km gap remains between the two faults. The 2003 fault does not reach the surface and its upper edge is at a depth of 3.5 ± 1 km. No evidence is found of slip south of the Lefkada Island as suggested by some seismological studies.

Keywords: Earthquake dynamics, Seismicity and tectonics, Radar interferometry, Lefkada

1. Introduction

Greece is the country with the highest seismicity in Europe. The main crustal deformations occur along the Hellenic Arc, as a result of the subduction of the African Nubian plate

beneath the Aegean plate (Le Pichon and Angelier, 1979; Ganas and Parsons, 2009a; Pérouse et al., 2012). The Central Ionian region (Fig. 1) is one of the most active areas of shallow seismicity in Greece (Benetatos et al., 2007) with an estimated full seismic coupling according to Chousianitis et al. (2015). The Central Ionian Islands, Lefkada, Cephalonia, Zakynthos, are located on the Aegean Plate between the Apulia – Eurasia continental collision to the north and oceanic subduction to the south, with intensive surface deformations due to ENE-WSW shortening (Ganas et al., 2013) with earthquake than can reach or exceed magnitude 7 like in 1953 or 1983 (Papazachos and Papazachou, 1997). The plate boundary in the Central Ionian Sea is defined by a major, right-lateral, strike-slip fault, the Cephalonia Transform Fault (CTF) which is located at the western termination of the Hellenic subduction zone, and is characterised by a bathymetric trough exceeding 3000 m depth. Strike-slip faulting prevails in a large area to the east of the CTF reaching the western boundaries of the Gulf of Corinth (Kiratzi et al., 2008; Ganas et al., 2009b; Serpetsidaki et al., 2014; Briole et al., 2015; Chousianitis et al., 2015).

In terms of geology, the Ionian Islands are built with sedimentary rocks, mainly carbonates, belonging to the so-called external Hellenides (Jacobshagen 1979; Underhill 1989). In particular, the boundary between the two different geological zones, called Ionian and Paxos, runs through this region and outcrops onshore Lefkada, forming the noteworthy Ionian Thrust which is assumed to be the westernmost limit of External Hellenides chain (Lagios et al., 2007). The main part of the Lefkada Island is made of a carbonate sequence of the Ionian zone, while the SW part of the island consists of limestone of Paxos geological zone (Bornovas 1964; Pavlides et al., 2004).

This tectonic regime predetermines the high seismic activity in the area of Lefkada Island. The island was affected indeed by several significant events in the past (Table 1). The two most recent strong earthquakes are the M_w = 6.2 2003 August 14 earthquake analyzed in this paper and the recent Mw = 6.5 2015 November 17 earthquake (Ganas et al., 2016; Chousianitis et al., 2016, Sokos et al., 2016). Both earthquakes occurred offshore the western coast of Lefkada Island, causing severe damages around the whole island.

2. Seismicity in the area and Lefkada fault location

According to the historical documentation of the last centuries several strong earthquakes occurred since the 17th century in the area of Lefkada Island. During the instrumental era five events with magnitude higher than 6 were recorded: one in 1914, two in 1948 (Fig. 2, Table 1), the 2003 event studied here, and the recent earthquake of 2015.

Taking into account 23 microseismic events recorded with portable seismographs by Hatzfeld et al. (1995) during a 7-week experiment in the summer of 1989, available macroseismic data, as well as the bathymetry change to a NNE direction northern of Cephalonia Island, Louvari et al. (1999) identify an active seismic segment of the CTF offshore west of the coast of Lefkada. The authors suggest that this northern segment strikes in a NNE-SSW direction, dips to ESE, has strike-slip motion combined with a small thrust component (Table 2), and has a length of ~40 km starting from the northern part of the Cephalonia Island. They interpret the thrust component of the M = 5.8 1973 November 4 earthquake (Baker et al., 1997) as an indication of the junction of the Albanian thrust belt with the Lefkada segment at the northern end of the CTF. Pavlides et al. (2004) assumes a division of Lefkada segment into two smaller segments separated by Sesoula Islet, west of Lefkada, striking at different directions, NNE-

SSW and NE-SW respectively for northern and southern sub-segment and behaving independently.

3. The 2003 August 14 earthquake

On 2003 August 14 at 05:15 GMT a $M_w = 6.2$ earthquake occurred offshore the western coast of Lefkada Island causing considerable damages (Fig. 3) in several settlements, all harbours and the road network, as well as landslides, rock falls, soil liquefaction, subsidence, ground cracks, especially along the north-western part of the island (Katopodi and Iosifidou, 2004; Papathanassiou et al., 2005; Pavlides et al., 2004).

A maximum intensity of VIII in the town of Lefkada was observed, while elsewhere in the island the intensity ranged from V to VII (Papadopoulos et al., 2003; Papathanassiou et al., 2005). The character and location of the damages are similar to those related to the previous strong earthquakes of similar magnitude in the area. Compared to the past events, the intensity decreased from X-XI, possibly due to the strict construction rules established after the last destructive earthquake of 1948. Nevertheless, ~120 houses were destroyed almost half of the buildings of the island were damaged in different degree (Pavlides et al., 2004).

Up to 2003 August 31 more than 470 aftershocks ($M > 1.5$), concentrated in two clusters, were recorded by the Patras Seismological Laboratory (Fig. 4), the strongest of which ($M_s = 5.25$) occurred eleven hours after the main shock. Papadopoulos et al. (2003), Karakostas et al. (2004) and Papadimitriou et al. (2006) consider the southern cluster, located close to the north-western coast of Cephalonia Island, rather representing a triggered seismicity on the Cephalonia segment, due to stress increase from the main shock, than typical aftershock activity, and it has to be noted that the same area was also activated after the 2014 Cephalonia sequence. On the contrary, Benetatos et al. (2005; 2007), Zahradník et al. (2005), Saltogianni and Stiros (2015), Sokos et al. (2016) suggest a complicated fault geometry of Lefkada segment, with two main sub-events and segmentation of the rupture in a double cluster. According to this latter group of authors, the multiple source character of the main shock is represented by two main sub-events along a N12°E to N20°E (depending on the authors) line that ruptured Lefkada segment from north to south (Table 2, Fig. 4). The two sub-events are separated in time and space at 14 s and ~40 km, respectively, have strike-slip focal mechanisms and induced concentration of aftershocks in two clusters with mainly strike-slip character along the NE-SW trending fault segment (Fig. 4). Thrust and reverse faulting mechanisms also detected, mostly in the north and mainland parts of the island, indicate possible activation of faults in adjacent areas, as the Ionian thrust zone.

The present investigation is concentrated on the deformations in the area of the main shock (or first sub-event) and the following sequence of aftershocks on the Lefkada Island (Fig. 4).

4. InSAR processing and analysis

In the catalogue of the European Space Agency (ESA), for the period between January 2003 and January 2008, we found 13 ascending and 20 descending ENVISAT/ASAR (C-band) passes from track 458 and track 322 respectively, over the area of interest (Fig. 5). In both cases of satellite viewing, only one of these scenes is pre-seismic: 2003 March 21 for the

ascending and 2003 June 25 for descending (Table 5). This limits the generation of co-seismic pairs with only one master image.

In spite of this limitation, the choice of the scenes used in our investigation is made in such a way that the image pairs formed have perpendicular baselines less than 200 m with respect to the pre-seismic image. This requirement is valid for six ascending images, which form 6 ascending co-seismic and 15 ascending post-seismic interferometric pairs (Fig. 6, Table 4 and Table 5), and 8 descending scenes, forming 8 co-seismic and 23 post-seismic interferograms (Table 4 and Table 5).

Standard processing flow of differential (2-pass) method was followed to generate the interferograms, using the Jet Propulsion Laboratory/California Institute of Technology open source package ROI_PAC 3.0 (Rosen et al., 2004). The raw images (level 0) were provided by ESA as well as the Doris precise orbit files, used for removing the orbital effects. To eliminate the topographic effect, a simulated interferogram is generated from the SRTM digital elevation model (DEM) version 4 (Jarvis et al., 2008). This DEM has 90 m resolution and a nominal vertical error of less than 16 m. Nevertheless, thorough studies conducted by Mouratidis et al. (2010) indicate that the actual absolute and relative errors (standard deviation) are well bellow 10 m. Multilooking (4 looks in range and 20 looks in azimuth) was applied to minimize the loss of coherence and reduce the speckle noise in the produced interferogram.

With this operation, the original pixel size of 7.8 m in range and 4.6 m in azimuth was averaged to 31.2 m and 91.4 m respectively. The Goldstein-Werner filter (Goldstein and Werner, 1998), optional in ROI_PAC package, was applied in the final stage of processing to improve the quality of the interferogram. The results are geo-referenced to the coordinate system of the used DEM (GCS/WGS84). Tacking into account the nominal accuracy of the DEM (h_{DEM} = 16 m) and the altitude of ambiguity (h_a) for each interferogram, the maximum expected error due to the topography is calculated (Table 4).

A main problem in our interferogram processing is the fact that the ENVISAT/ASAR images are C-band, so the presence of vegetation has a strong influence on the coherence. The whole island is indeed dense vegetated mainly with olive groves and pine forests, especially to the east and south. This is probably the reason for coherence loss in all produced interferograms (see the Appendixes). To illustrate better the regions where the received signal is more reliable, a map of coherence is produced (Fig. 7) on a basis of all processed ascending interferograms. The value of the coherence for every pixel from the map is calculated first as a mean between the values of its neighbouring in the respective image and second the results of the corresponding pixels from all interferogram are averaged. In this way the reoccurrence in time and space of stable backscattered signal for each pixel is characterized. The areas with better scattering capabilities on the produced map correspond to the not overgrown Stavrota mountain (in the centre of the island), Kalavros to the north, big settlements like town of Lefkada and Preveza, and plain areas around Voulkaria Lake in mainland north-eastern from the island.

Examining the ascending data set, the interferogram which comprises the shortest time span (174 days) and has only 35 m perpendicular baseline, namely 21.03.2003-12.09.2003 (interferogram No 1 – *ifg*1 in Table 4), is expected to have the best quality. Lagios et al. (2007) analyse exactly this interferometric pair and describe 1 fringe in the northernmost part of the island and 2 fringes in the western part. However, in the current investigation a wider

set of data is studied and it is found that the interferogram *ifg*5 (21.03.2003-5.11.2004), which covers a longer period (592 days) and has a larger perpendicular baseline (88 m), shows much better quality (Fig. 9 left) than the interferogram *ifg*1 (APPENDIX A). The fringes of the 21.03.2003-5.11.2004 pair are more sharpened, while the interferogram pattern of pair *ifg*1 is strongly deformed. A possible explanation about this difference could be the lower percentage of humidity and cloudiness during the acquisition of the slave image in the pair *ifg*5 (Table 5), than the same weather characteristics in the day of the slave image of pair *ifg*1. Although, the local disturbances and the local temporal differences in humidity level have more important role in the phase de-correlation, even the homogeneous change in the atmosphere (pressure, humidity, and temperature) can be revealed by a contrasted relief, which modulates the thickness of the troposphere that the signal must cross (Massonnet and Feigl, 1998) since the topography induces tropospheric delays. In the case of Lefkada Island the elevation varies from sea level to 1160 m in the central part of the island, which is roughly the place where the strongest distortions occur. From the data of this study and other recent data over Lefkada Island, we estimate that tropospheric disturbances could be of ~1 C_band fringe (28 mm of delay) over the island.

No post-seismic deformation is observed in our interferograms (APPENDIX B) but we cannot exclude the presence of a small amount of such deformation as it has been observed elsewhere for strike-slip events of similar magnitude (e.g. Bürgmann et al., 1997).

The ascending co-seismic interferogram with the best quality (*ifg*5), covering the time period between 2003 March 21 and 2004 November 5 (Fig. 9 left), shows at least 2 fringes in the western part of the island. Since one fringe is equal to half the wavelength, which for ENVISAT C-band is 28 mm, then these two fringes are equal to 56 mm of deformation of the crust in the satellite line of sight (LoS). A verification in Table 4 shows that a very small part of detected fringes could be attributed to errors due to the topography – 4 mm, which is only 1/7 of the fringe.

In the case of descending co-seismic set of data, the deformations after the occurrence of the strong earthquake are detected with significantly lower quality, mainly because of the look direction of the satellite towards the highest mountains, so that the deformation pattern appeared distorted. The descending co-seismic interferogram with the best quality is the one with the smallest temporal separation (*ifg*22 – Fig. 8) and has a perpendicular baseline of 118 m (Table 4).

5. Modelling

The modelling and interpretation of the interferograms is made in three successive phases: first we model the best ascending wrapped interferogram only, then we analyze the stacks of unwrapped ascending and descending interferograms, and finally we perform a joint inversion of ascending and descending data.

The fringes in the best ascending interferogram are sampled to 34 points which we found sufficient to account for the level of quality of the data (using more sample points leads to the same model). One value of slant range displacement is sampled every ~1 km (Fig. 9 left - inset). The descending interferograms are not used in this first analysis, due to their lower quality. The Harvard CMT solution is used as initial parameters in inversion procedure (Table 2) fixing the strike angle to 18° and dip angle to 59°. The applied inversion algorithm was

developed by Briole et al. (1986), it is based on the least-square minimization approach proposed by Tarantola and Valette (1982). The Okada (1992) formulation for rectangular-plane source in uniform elastic half-space is adopted for the dislocation source. The parameters of the best fitting model (Fig. 9 right) are listed in Table 3. The epicentre is located at the SW end of our modelled fault plane. If this is so the geodetic epicentre is offset by about 6 km to the NE of the NOA epicentre.

The fringes obtained in the synthetic interferogram are in good agreement with the observed ones, evident also by the residuals between the phase values of the fringe points from the model and the same points in the real interferogram. The value of the mean is -0.9 mm and the root-mean-square (r.m.s.) residual is 2.3 mm i.e. only 1/12 part of a fringe. The concordance of the proposed modelled fringe points with the observed ones is manifested by the distribution of the residual (Fig. 10 left), which is close to the normal one. Additionally, since the number of the points is relatively small, a normal probability plot is presented (Fig. 10 right). This plot shows some outliers in both ends of the data set but still confirms the normal distribution of the residuals.

In order to confirm the reliability of the proposed model of the fault, a series of inversions are conducted with varying dip and length of the fault, taking into account the values proposed by previous studies (Fig. 11). In both cases, while the different values for the dip and length are tested, all the other parameters are left fixed. This investigation of the confidence of these parameters shows that the best fitting model would be achieved at dip of 60° and length of the faulting segment of 16 km. However, the r.m.s. difference for a model with dip of 60° and 59°, like the value proposed here, on the basis of Harvard CMT solution, is only 0.4 mm (1/70 of the fringe), which is not significant.

The sensitivity of the model to the dip alteration is expressed by “pressing” of the fringe’s shape. In the case investigated here, the mean part of the outer fringe is not clearly outlined. To increase the quality of the interferometric pattern and to improve the fringe shape, an interferogram averaged from all the six co-seismic ascending interferograms is produced. As a first step all of them are unwrapped using the SNAPHU software (Chen and Zebker, 2002) (APPENDIX A). The stacking of all co-seismic ascending interferograms and the backward wrapping (Fig. 12d) of the phases increased in some aspect the quality of the single wrapped picture (Fig. 12a). The resulting field of deformation of the single interferogram (Fig. 12b) shows maximum displacement toward the satellite in the range of 60 mm. The stacking of the available interferograms (Fig. 12c) narrows the area of deformations and decreases its value to ~50 mm.

When the re-wrapped interferogram is superimposed over the topography (Fig. 12e), high dependency of the local relief is revealed. In spite of the more homogeneous field of deformation which is represented by the unwrapped stacked interferogram compared to the interferogram with the best quality, the averaged unwrapped pattern also combines all defects of the interferograms used in the stacking. This is illustrated by cross-sections through the unwrapped interferograms in Fig. 13. The A’-A” profile is traced parallel to the strike of the fault and is presented in the upper part of the figure, while the B’-B” profile passes through the island and represents the area with the most pronounced crust deformation (bottom of the figure). The corresponding local relief is plotted to the bottom of the profiles.

It is seen how a processing error during the unwrapping procedure (APPENDIX A) caused distortion of the field of deformation of *igf*4 showed in the profile by dotted line (UWRI4 –

unwrapped real interferogram *ifg*4). If this interferogram is excluded of the averaging, the middle part of the interferogram becomes more uniform (red line, UWSRI – unwrapped **s**tacked **r**eal **i**nterferogram), but the level of deformation in the outlying areas vary significantly in the A'A" profile. The abrupt change of the deformation line appeared in a place of a steep topographic depression at the boundary between the Ionian and Paxos geological zones, which could influence strongly the unwrapping process. Nevertheless, the averaged interferogram shows high level of concordance to the modelled one (MI in Fig. 13), even better that the single interferogram used for the modelling (UWRI5). The received field of crustal deformations, excluding the wrong *ifg*4, shows a maximum in the range of ~60 mm towards the satellite (Fig. 12f). The shift between the real and the modelled data in the right part of the A'A" profile is again a consequence of the unwrapping defect in the area of the Ionian Thrust like in the case of *ifg*4 but in the opposite direction. If the real data in this part of the interferograms are shifted with the amount of exactly one fringe downward they will correspond to the model. On the other hand, the left part of the B'B" profile shows a big difference between the data and the model. Since the images used for producing these interferograms are ascending, this area follows in the shadow of the high mountain in the centre of the island looked from the satellite. Therefore, the signal in this area is in fact an incoherent noise and the unwrapping procedure performs false information about the deformation in this area. None conclusions can be made in this situation about the reliability of the model in this area.

In order to find another confirmation about the agreement between the fields of deformation revealed by the interferograms and predicted by the model, a comparison on a pixel level is performed. The examination of the residuals between the real and the synthetic deformation interferograms (Fig. 14) displays a high degree of correspondence between both patterns, which is confirmed also by the histogram of the residuals (Fig. 15). It manifests very close to the normal distribution, shifted by the mean value of 3.4 mm. The r.m.s. for the entire examined pattern is 10.5 mm.

The stacking procedure is applied also to the descending set of data, so that the field of deformation from the other point of satellite view could be gained. The stacked re-wrapped interferogram shows one clear fringe (Fig. 16), but in the rest of the interferogram still high level of noise presents (APPENDIX C).

Nevertheless, the averaged descending unwrapped interferogram will be used, together with the ascending result, in a theoretical determination of the horizontal and vertical components of the field of deformations. To define two of the three components of the LoS displacement, an assumption for the third one should be adopted. Here, the northern component is equalised for both satellite viewings, thus the displacement in up and east direction (Fig. 17) is extracted using the parameters of the satellite geometry (Hanssen, 2001). The resulting pattern shows a maximum vertical displacement of the Earth's crust in the range of ~50 mm in the western-central part of the island and eastward displacements in the western coast in the maximum range of ~60 mm.

Finally we make a model by jointly inverting ascending and descending data. The combination of ascending and descending observations is potentially powerful to constrain some of the fault parameters, in particular depth, location of the fault in the east-west axis, and dip-slip component of motion. We use the two best interferograms (ascending *ifg5* and descending *ifg22*, see Table 4), with the 34 picked values on two fringes visible on the ascending interferogram (those already used before) and 20 picked values on the only clear

fringe of the descending one. The ratio 20/34 gives less weight to the descending data in the inversion. This is consistent with the fact that, given its lower coherence, we are less confident in this data than in the ascending one. Starting with the parameters of our preferred model (IL16, Table 3) we first leave free all fault parameters in the inversion. Only two of the fault parameters show significant changes: the depth of the upper edge of the fault that is estimated deeper, at 4.5 km instead of 2.5 km, and the east coordinate of the fault that moves westward in a correlated manner with the fault depth. The other parameters are not significantly affected by the addition of the descending data. Another benefit of the joint inversion of ascending and descending data is the fact that, because of the existence of two opposite LoS, it is possible to seek for an optimum in the common mode offset to apply to the picked value of the fringes. We tune the picked value so as to minimize the post-fit residuals at a minimum value of 9 mm, and Table 7 and Table 8 contain the location and observed and modelled value of our picked fringe points. In all inversions the component of dip-slip on the fault plane remains close to zero, ranging from -18 mm (reverse) when the upper fault depth was assigned to be 5 km to +21 mm (normal) when the upper fault depth was assigned to be 4 km. Table 9 contains the value of the two preferred models. In summary, the two main constraints provided by the combination of the ascending and descending data are the following: no significant component of dip-slip on the fault, an upper limit of the fault possible deeper (4.5 km instead of 2.5 km with ascending only).

6. Discussion and conclusions

We examine fault size, geometry and its relation to earthquake magnitude and how this relates to the historical seismicity record (Table 1). Our geodetic solution (Fig. 9) indicates that the rupture length is ~16 km, a value close to that predicted by the empirical relationship of Wells and Coppersmith (1994) (see Table 6), and much less than those predicted by the equations of Papazachos and Papazachou (1997) and Konstantinou et al. (2005). The 2003 Lefkada event occurred along one fault segment plane dipping to the east as suggested by the linear inversion of the InSAR fringes. The earthquake was followed by numerous aftershocks on neighbouring fault planes that are characterised as capable to produce moderate events (Karakostas and Papadimitriou, 2010). The geodetically determined fault size is about half the length of the Lefkada plate boundary segment defined by seismological data by Louvari et al. (1999). In addition, Papadopoulos et al. (2003) have suggested that offshore earthquakes near Lefkada follow the characteristic earthquake model, i.e. slip distribution and earthquake magnitude are roughly constant. Our results indicate that, the 2003 earthquake ruptured only the northern portion of the 50-km Lefkada segment of CTF, which is about 16 km long. Assuming that the Lefkada segment of CTF comprises two seismic segments then, this segmentation model predicts rupture lengths of the order of 15-20 km and maximum earthquake magnitudes in the range 6.2-6.5. This suggestion has important consequences for the seismic hazard of the area, as the earthquakes expected offshore Lefkada may reach M_w = 6.5 like the 2015 November 17 southern Lefkada earthquake (Ganas et al., 2016). For both the 2003 earthquake (this study; Fig. 9 right) and the 2015 one (Ganas et al. 2016; Fig. 4), InSAR constrains well the spatial extend of the rupture along the axis of the CTF. We infer from the two studies that a 10-15 gap remains between the 2003 and the 2015 fault planes. A gap of such length corresponds to a potential earthquake of Mw ~ 5.7-6. Some authors (Saltogianni and Stiros, 2015; Sokos et al., 2016) have suggested that the 2003 event also broke a fault segment south of the 2015 fault, in front of the northern Cephalonia, in a very unusual manner. We found no evidence of such southern segment in our 2003 interferograms. Moreover, this hypothetical jump of the 2003 rupture over the 2015 fault should also jump

over the 10-15 gap located between the 2003 and 2015 faults. This corresponds to a distance of ~40 km between the second hypothetical sub-event and the main shock of 2003, itself well modelled from the InSAR data and with a good agreement between geodetic and seismological moments.

The fault model we propose has a geodetic moment $M_o = 3.6\ 10^{18}$ N m which corresponds to $M_w = 6.3$, greater than the seismic moment reported by the Harvard CMT solution which is $M_o = 2.98\ 10^{18}$ N m or $M_w = 6.2$. The difference might be due to the influence of the two larger shallow aftershocks, that occurred the same day as the main shock, with $M_w = 5.1$ and $M_w = 5.5$ respectively.

The interferometric pattern, produced by ENVISAR/ASAR images, defines field of deformations caused by the 2003 Lefkada earthquake, in the range of 60-70 mm in the line of sight of the satellite. An attempt to determine the horizontal and vertical component of displacement is performed. An uplift of about 50 mm in the central area of deformation is calculated and deformations with eastward direction in the range of 60 mm in the western coast of the island are estimated.

The 2003 fault does not reach the surface. Its upper tip is located at a depth comprised between 2.5 km (using ascending data only) and 4.5 km (using a combination of ascending and descending). This is much deeper that the depth of the upper tip of the 2015 fault, estimated to be ~1 km around the northern end of the fault according to Ganas et al. (2016). The mode and timing of the deformation between that depth and the surface requires further analysis. Is the uppermost part of the crust deforming continuously during the seismic cycle in that segment or is there a possibility of very shallow and strong earthquakes? And why is the 2015 rupture shallower? In addition to SAR interferometry (which is insufficient for sampling long time periods in areas of poor coherence), dense and permanent GPS will be important to decipher the spatio-temporal behaviour of the uppermost crust along the Cephalonia Transform Fault. The combination of ascending and descending InSAR observations indicates that there is no significant component of dip-slip on the fault of this 2003 earthquake.

Acknowledgements

The ENVISAT/ASAR images used in the present study were provided by the European Space Agency in the framework of the Category–1 project ID 4484: “Investigation of the south-eastern part of the Sofia complex graben (Bulgaria) by InSAR and GPS methods with comparative analysis with the Lefkada Island (Greece)”. The study was realised in the framework of the bilateral project RILA (3/29, 2007-2008) between the Ministry of Education, Youth and Science of Bulgaria and Ministry of National Education, France. The Generic Mapping Tools system (Wessel and Smith, 1998) was used to plot some of the figures. The authors would like to thank Hélène Lyon-Caen, Marie-Pierre Doin, Efthimios Sokos, Krassimir Matev and Dragan Chobanov for their invaluable help. We thank Ziyadin Çakır for his review and comments.

References

Amante, C., Eakins, B.W., 2009. ETOPO1 1 Arc-Minute Global Relief Model: Procedures, Data Sources and Analysis, NOAA Technical Memorandum NESDIS NGDC-24, 19 pp.

449 Baker, C., Hatzfeld, D., Lyon-Caen, H., Papadimitriou, E., Rigo, A., 1997. Earthquake
450 mechanisms of the Adriatic Sea and western Greece. Geophys. J. Int., 131, 559-594.
451 Barrier, E., Chamot-Rooke, N., Giordano, G., 2004. Geodynamic map of the Mediterranean,
452 sheet 1: Tectonics and Kinematics, CGMW, France.
453 Benetatos, C., Kiratzi, A., Roumelioti, Z., Stavrakakis, G., Drakatos, G., Latoussakis, I., 2005.
454 The 14 August 2003 Lefkada island (Greece) earthquake: Focal mechanisms of the
455 mainshock and the aftershock sequence, J. Seismol, 9, 171-190.
456 Benetatos, C., Dreger, D., Kiratzi, A., 2007. Complex and Segmented Rupture Associate with
457 the 14 August 2003 M_w 6.2 Lefkada, Ionian Islands, Earthquake. Bull. Seism. Soc. Am.,
458 97(1B), 35-51.
459 Bornovas, J., 1964. Géologie de l'île de Lefkade. Geol. Geophys. Res. (Special Publication by
460 Greek Geological Survey), 10(1).
461 Briole, P., De Natale, G., Gaulon, R., Pingue, F., Scarpa R., 1986. Inversion of geodetic data
462 and seismicity associated with the Friuli earthquake sequence (1976 – 1977). Annales
463 Geophysicae, 4, 481-492.
464 Briole, P., Elias, P., Parcharidis, I., Bignami, C., Benekos, G., Samsonov, S., Kyriakopoulos,
465 C., Stramondo, S., Chamot-Rooke, N., Drakatou, M.L., Drakatos, G., 2015. The seismic
466 sequence of January–February 2014 at Cephalonia Island (Greece): constraints from SAR
467 interferometry and GPS, Geophys. J. Int., doi: 10.1093/gji/ggv353.
468 Bürgmann, R., Segall, P., Lisowski, M., Svarc, J., 1997. Postseismic strain following the 1989
469 Loma Prieta earthquake from GPS and levelling measurements, J. Geophys. Res.,
470 102(B3), 4933-4955, doi:10.1029/96JB03171.
471 Chen, C.W., Zebker, H.A., 2002. Phase unwrapping for large interferograms: Statistical
472 segmentation and generalized network models, IEEE Transactions on Geoscince and
473 Remote Sensing, 40, 1709-1719.
474 Chousianitis, K., Ganas, A., Evangelidis, C.P., 2015. Strain and rotation rate patterns of
475 mainland Greece from continuous GPS data and comparison between seismic and
476 geodetic moment release, J. Geophys. Res. Solid Earth, 120, doi:10.1002/2014JB011762.
477 Fokaefs, A., Papadopoulos G.A., 2004. Historical earthquakes in the region of Lefkada island,
478 Ionian sea – estimation of magnitudes from epicentral intensities. Bull. Geol. Soc. Gr.
479 (Proc. 10th Intl. Conf. Thessaloniki), 36, 389-1395.
480 Ganas, A., Parsons T., 2009a. Three-dimensional model of Hellenic Arc deformation and
481 origin of the Cretan uplift. J. Geophys. Res., 114, doi: 10.1029/2008JB005599.
482 Ganas, A., Serpelloni, E., Drakatos, G., Kolligri, M., Adamis, I., Tsimi, C., Batsi, E., 2009b.
483 The Mw 6.4 SW-Achaia (Wsetern Greece) Earthquake of 8 June 2008: Seismological,
484 Field, GPS Observations, and Stress Modelling. J. Earthquake Engineering, 13(8), 1101-
485 1124.
486 Ganas, A., Marinou, A., Anastasiou, D., Paradissis, D., Papazissi, K., Tzavaras, P., Drakatos
487 G., 2013. GPS-derived estimates of crustal deformation in the central and north Ionian
488 Sea, Greece: 3-yr results from NOANET continuous network data, J. Geodyn., 67, 62-71.
489 Ganas, A, Elias, P, Bozionelos, G, Papathanassiou, G, Avallone, A, Papastergios, A,
490 Valkaniotis, S, Parcharidis, I, Briole, P, 2016. Coseismic deformation, field observations
491 and seismic fault of the 17 November 2015 M = 6.5, Lefkada Island, Greece earthquake,
492 Tectonophysics, ISSN 0040-1951,http://dx.doi.org/10.1016/j.tecto.2016.08.012
493 Geological map of Greece – Lefkas (1963). Institute for geology and subsurface research.
494 Goldstein, R.M., Werner, C.L., 1998. Radar interferometry filtering for geophysical
495 applications. Geophys. Res. Lett., 25 (21), 4035-4038.
496 Goldsworthy, M., Jackson, J., Haines, J., 2002. The continuity of active fault system in
497 Greece. Geophys. J. Int., 148, 596-618.

Hanssen, R., 2001. Radar Interferometry: Data Interpretation and Error Analysis. Ser.: Remote Sensing and Digital Image Processing, Volume 2. Kluwer Academic Publishers, Dordrecht, The Netherlands, pp 308.

Hatzfeld, D., Kassaras, I., Panagiotopoulos, D., Amorese, D., Makropoulos, K., Karakaisis, G., Coutant, O., 1995. Microseismicity and strain pattern in northwestern Greece. Tectonics, 14(4), 773-785.

Hollenstein, C., Müller, M., Geiger, A., Kahle, H.G., 2008. GPS-Derived Coseismic Displacements Associated with the 2001 Skyros and 2003 Lefkada Earthquakes in Greece. Bull. Seism. Soc. Am., 98(1), 149-161.

Jacobshagen, V., 1979 Structure and geotectonic evolution of the Hellenides. Proc. VI Colloq Aegean Region Athens 1977, IGMR, Athens, pp 1355-1367.

Jarvis, A., Reuter, H.I., Nelson, A., Guevara, E., 2008. Hole-filled seamless SRTM data V4, International Centre for Tropical Agriculture (CIAT), available from http://srtm.csi.cgiar.org.

Karakostas, V., Papadimitriou, E., 2010. Fault complexity associated with the 14 August 2003 M_w6.2 Lefkada, Greece, aftershock sequence. Acta Geophysica, 58 (5), 838-854.

Karakostas, V., Papadimitriou, E., Papazachos, C., 2004. Properties of the 2003 Lefkada, Ionian Islands, Greece, Earthquake Seismic Sequence and Seismicity Triggering. Bull. Seism. Soc. Am., 94(5), 1976-1981.

Katopodi, I.,Iosifidou, K., 2004. Impact of the Lefkada earthquake (14-08-2003) on marine works and coastal regions. Proc. The 7th Panhellenic Geographical Conference of the Hellenic Geographical Society (7PGC/HGS), Mytilene, Greece, 1-8.

Kiratzi, A., Sokos, E., Ganas, A., Tselentis, A., Benetatos, C., Roumelioti, Z., Serpetsidaki, A., Andriopoulos, G., Galanis, O., Petrou, P., 2008. The April 2007 earthquake swarm near Lake Trichonis and implications for active tectonics in Greece. Tectonophysics, 452, 51-65.

Konstantinou, K.I., Papadopoulos, G.A., Fokaefs, A., Orphanogiannaki, K., 2005. Empirical relationships between aftershock area dimentions and magnitude for earthquake in the Mediterranean Sea region. Tectonophysics, 403, 95-115.

Lagios, E., Sakkas, V., Papadimitriou, P., Parcharidis, I., Damiata, B.N., Chousianitis, K., Vassilopoulou, S., 2007. Crustal deformations in The Central Ionian Islands (Greece): Results from DGPS and DInSAR analyses (1995 - 2006). Tectonophysics, 444, 119-145.

Le Pichon, X., Angelier, J., 1979. The Hellenic arc and trench system: a key to the Eastern Mediterranean area, Tectonophysics, 60, 1-42.

Louvari, E., Kiratzi, A.A , Papazachos, B.C., 1999. The Cephalonia Transform Fault and its extension to western Lefkada Island (Greece). Tectonophysics, 308, 223-236.

Massonnet, D., Feigl, K., 1998. Radar interferomtry and its application to changes in the Earth's surface. Rev. Geophys., 36(4), 441-500.

Mouratidis, A., Briole, P., Katsambalos K., 2010. SRTM 3″ second DEM (versions 1, 2, 3, 4) validation by means of extensive kinematic GPS measurements: a case study from North Greece. Int. J. Remote Sensing, 31 (23), 6205-6222.

Okada, Y., 1992. Internal deformation due to shear and tensile faults in a half-space. Bull. Seism. Soc. Am., 82, 1018-1040.

Papadimitriou, E.E., 2002. Mode of Strong Earthquake Recurrence in the Central Ionian Islands (Greece): Possible Triggering due to Coulomb Stress Changes Generated by the Occurrence of Previous Strong Shocks. Bull. Seism. Soc. Am., 92(8), 3293–3308.

Papadimitriou, P., Kaviris, G. & Makropoulos, K., 2006. The Mw = 6.3 Lefkada earthquake (Greece) and induced stress transfer changes. Tectonophysics, 423, 73-82.

Papadopoulos, G., Karastathis, V., Ganas, A., Pavlides, S., Fokaefs, A., Orfanogiannaki, K., 2003. The Lefkada, Ionian Sea (Greece), shock (Mw 6.2) of 14 August 2003: Evidence

548 for the characteristic earthquake from seismicity and ground failures. Earth Planets Space,
549 55, 713-718.
550 Papathanassiou, G., Pavlides, S., Ganas, A., 2005. The 2003 Lefkada earthquake: Field
551 observations and preliminary microzonation map based on liquefaction potential index for
552 the town of Lefkada. Engineering Geology, 82, 12-31.
553 Papathanassiou, G., Pavlides, S., 2007. Using the INQUA scale for the assessment of
554 intensity: Case study of the Lefkada (Ionian Islands), Greece earthquake. Quaternary
555 International, 173-174, 4-14.
556 Papazachos, B.C., Papazachou, C.B., 1997. The earthquakes of Greece, Ziti Publication Co.,
557 Thessaloniki, 304 pp.
558 Papazachos, B.C., Papadimitriou, E.E, Kiratzi, A.A, Papazachos, C.B., Louvari, E.K, 1998.
559 Fault plane solutions in the Aegean and the surrounding area and their tectonic
560 implications. Boll. Geof. Teor. Appl. 39, 199–218.
561 Papazachos, B.C., P.E. Comninakis, G.F. Karakaisis, B.G. Karakostas, Ch.A. Papaioannou,
562 C.B. Papazachos, Scordilis, E.M., 2000. A Catalogue of Earthquakes in Greece and
563 Surrounding Area for the Period 550BC–1999 1. Publ. Geoph. Lab., Univ. of
564 Thessaloniki, 333 pp.
565 Pavlides, S.B., Papadopoulos, G.A., Ganas, A., Papathanassiou, G., Karastathis, V.,
566 Keramydas, D., Fokaefs, A., 2004. The 14 August 2003 Lefkada (Ionian sea) earthquake.
567 5th Int. Symp. On Eastern Med. Geology, Thessaloniki, 14 – 20 April, 2, 942-946.
568 Pérouse, E., Chamot-Rooke, N, Rabaute, A., Briole, P., Jouanne, F., Georgiev, I., Dimitrov,
569 D., 2012. Bridging onshore and offshore present-day kinematics of central and eastern
570 Mediterranean: implications for crustal dynamics and mantle flow, Geochem. Geophys.
571 Geosyst., 13 (9), doi : 10.1029/2012gc004289.
572 Rosen, P.A., Hensley, S., Peltzer, G., Simons, M., 2004. Update Repeat Orbit Interferometry
573 Package Released. EOS Trans. AGU, 85(5), 35.
574 Saltogianni, V., Stiros, S., 2015. A Two-Fault Model of the 2003 Leucas (Aegean Arc)
575 Earthquake Based on Topological Inversion of GPS Data, Bull. Seism. Soc. Am., 105(5),
576 doi: 10.1785/0120140355
577 Serpetsidaki, A., Elias, P., Ilieva, M., Bernard, P., Briole, P., Deschamps, A., Lambotte, S.,
578 Lyon-Caen, H., Sokos, E., Tselentis, G.A., 2014, New constraints from seismology and
579 geodesy on the Mw = 6.4 2008 Movri (Greece) earthquake: evidence for a growing strike-
580 slip fault system Geophys. J. Int., 198 (3), 1373-1386, doi:10.1093/gji/ggu212.
581 Sokos, E., Zahradnik, J., Gallovic, F., Serpetsidaki, A., Plicka, V., Kiratzi, A., 2016. Asperity
582 break after 12 years: The M_w6.4 2015 Lefkada (Greece) earthquake, Geophys. Res. Lett.,
583 43(12), 6137-6145, doi: 10.1002/2016GL069427
584 Tarantola, A., Valette, B., 1982. Generalized nonlinear inverse problem solved using the least
585 squares criterion. Reviews Geophys., 20, 219-232.
586 Underhill, J.R., 1989. Late Cenozoic deformation of the Hellenide foreland, western Greece,
587 Geol. Soc. Am. Bull., 101, 613-634.
588 Wells, D.L., Coppersmith, K.J., 1994. New empirical Relationships among Magnitude,
589 Rupture Length, Rupture Width, Rupture Area, and Surface Displacement. Bull. Seis.
590 Soc. Am., 88 (4), 974-1002.
591 Wessel, P., Smith, W.H.F., 1998. New improved version of the Generic Mapping Tools
592 released, EOS trans., AGU, 79 (47), 579.
593 Zahradník, J., Serpetsidaki, A., Sokos, E., Tselentis, G.A., 2005. Iterative Deconvolution of
594 Regional Waveforms and a Double-Event Interpretation of the 2003 Lefkada Earthquake,
595 Greece. Bull. Seism. Soc. Am., 95(1), 159-172.
596
597

FIGURES – FIGURE CAPTIONS

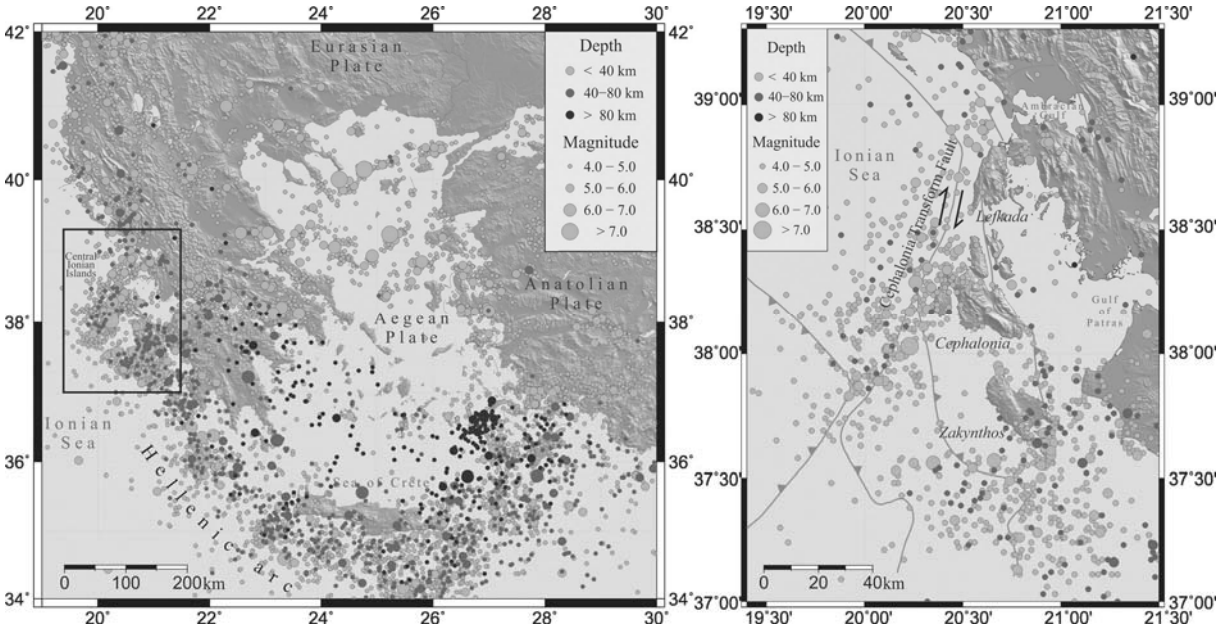

Fig. 1. Left: Seismicity (M>4) in the Eastern Mediterranean since 1973 according to USGS. Rectangle – the region of Central Ionian Islands. Right: Seismicity in the area of the Central Ionian Islands. Fault geometry is adapted from Barrier et al. (2004).

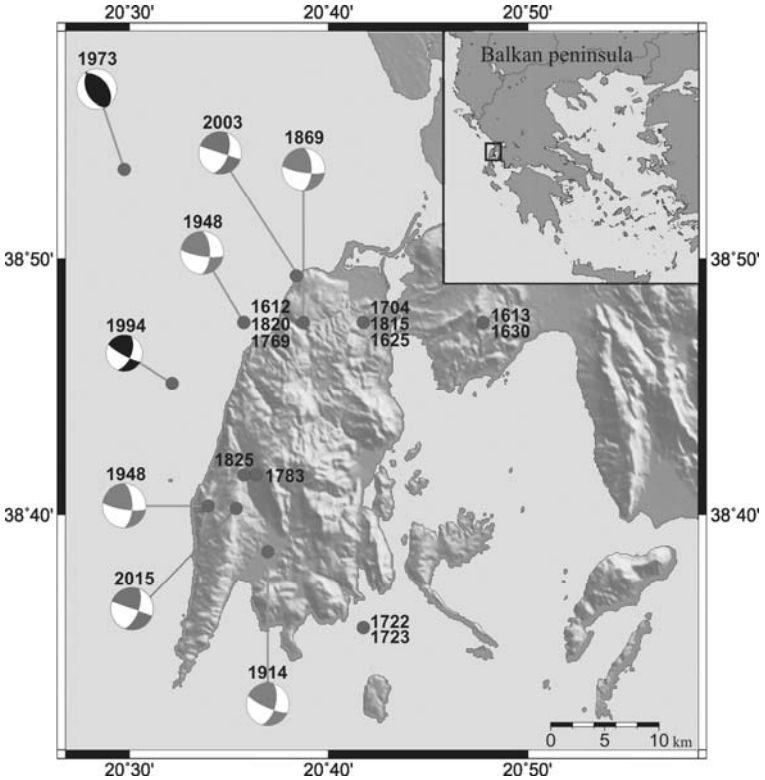

Fig. 2. Historical seismicity in the area of Lefkada Island according to Table 1. In inset the location of the Lefkada Island in Eastern Mediterranean. In grey, the mechanisms of strong historical events are marked, while in black – the mechanisms of most recent earthquakes even though they were of smaller magnitudes. The mechanisms of the 2003 and 2015 earthquakes are plotted in red.

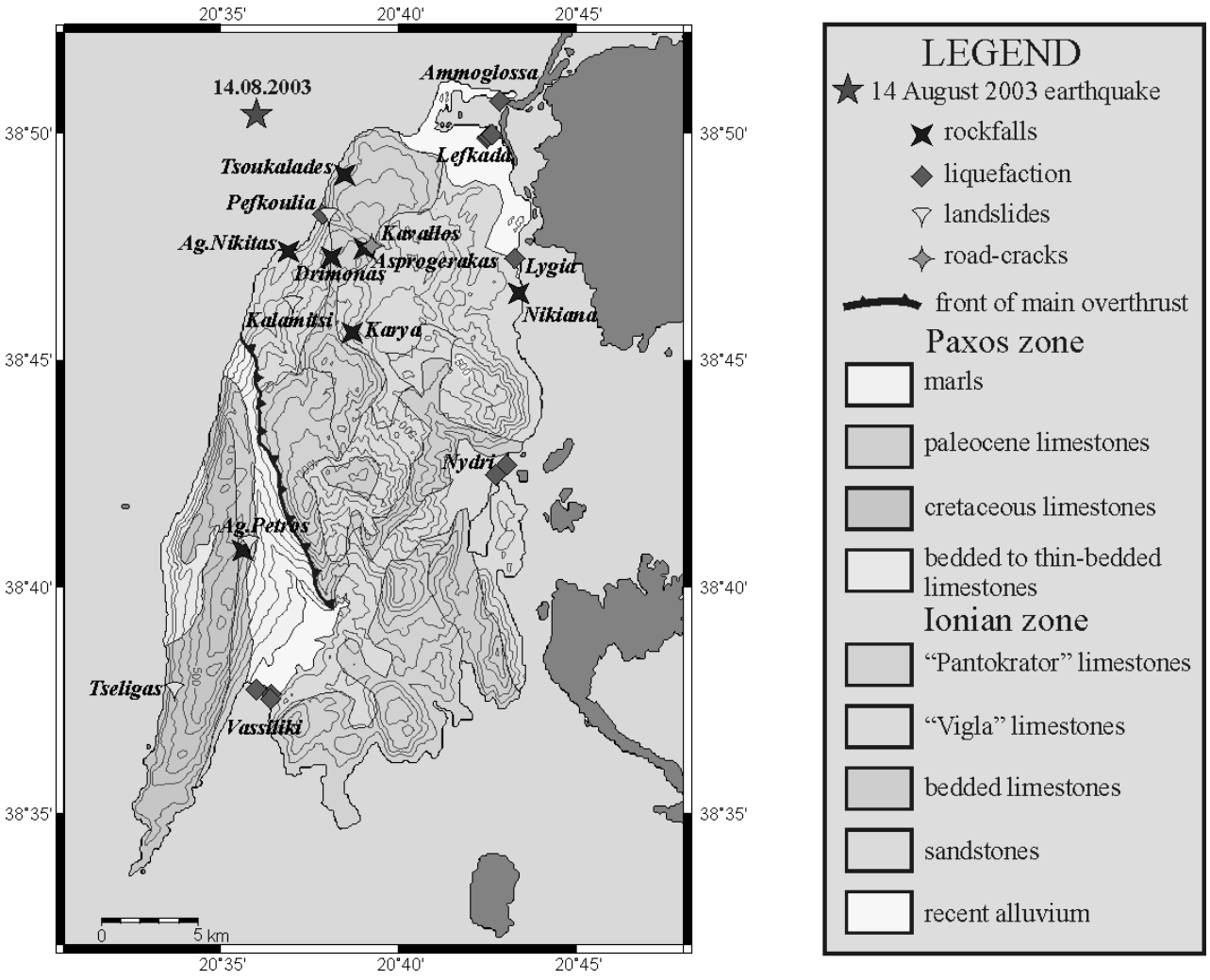

611
612

613 Fig. 3. Map of ground failures caused by the 14th August 2003 earthquake (after Pavlides et
614 al., 2004; Papathanassiou and Pavlides, 2007). On the background simplified geological map
615 of the Lefkada Island (Geological map of Greece 1963).

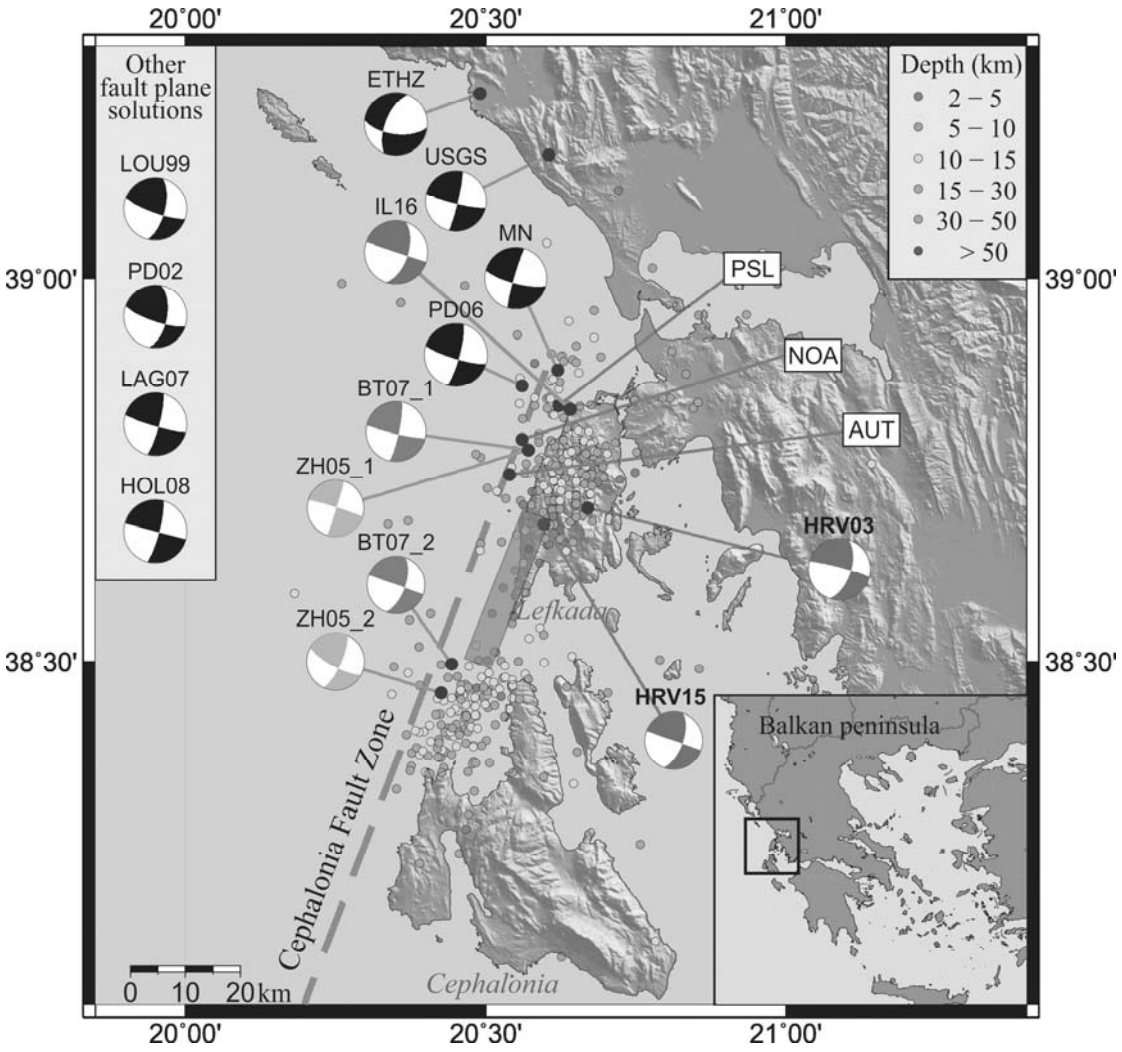

Fig. 4. The 14th August 2003 Lefkada earthquake from different sources (Table 2) – the notation is the same as the references notations in the table. Other fault plane solutions (Table 3) are also shown (the notation is the same as the references notations in the table): LOU99 – typical focal mechanism obtained by waveform modelling of micro-earthquakes; PD02 – stress evolutionary model; LAG07 – InSAR forward modelling; HOL08 – Okada model based on co-seismic GPS measurements. Aftershock sequence from PSL is introduced with coloured circles according to the depth. In the present investigation the Harvard solution for the 2003 event (in red – HRV03) is taken as a basic in inversion process. The final solution of our study is shown in brown (IL16) referred to the centre of the fault predicted by the fault model. The Harvard solution for the 2015 event is shown (HRV15) with relocated epicentre and modelled fault plane (red rectangle) from Ganas et al. (2016).

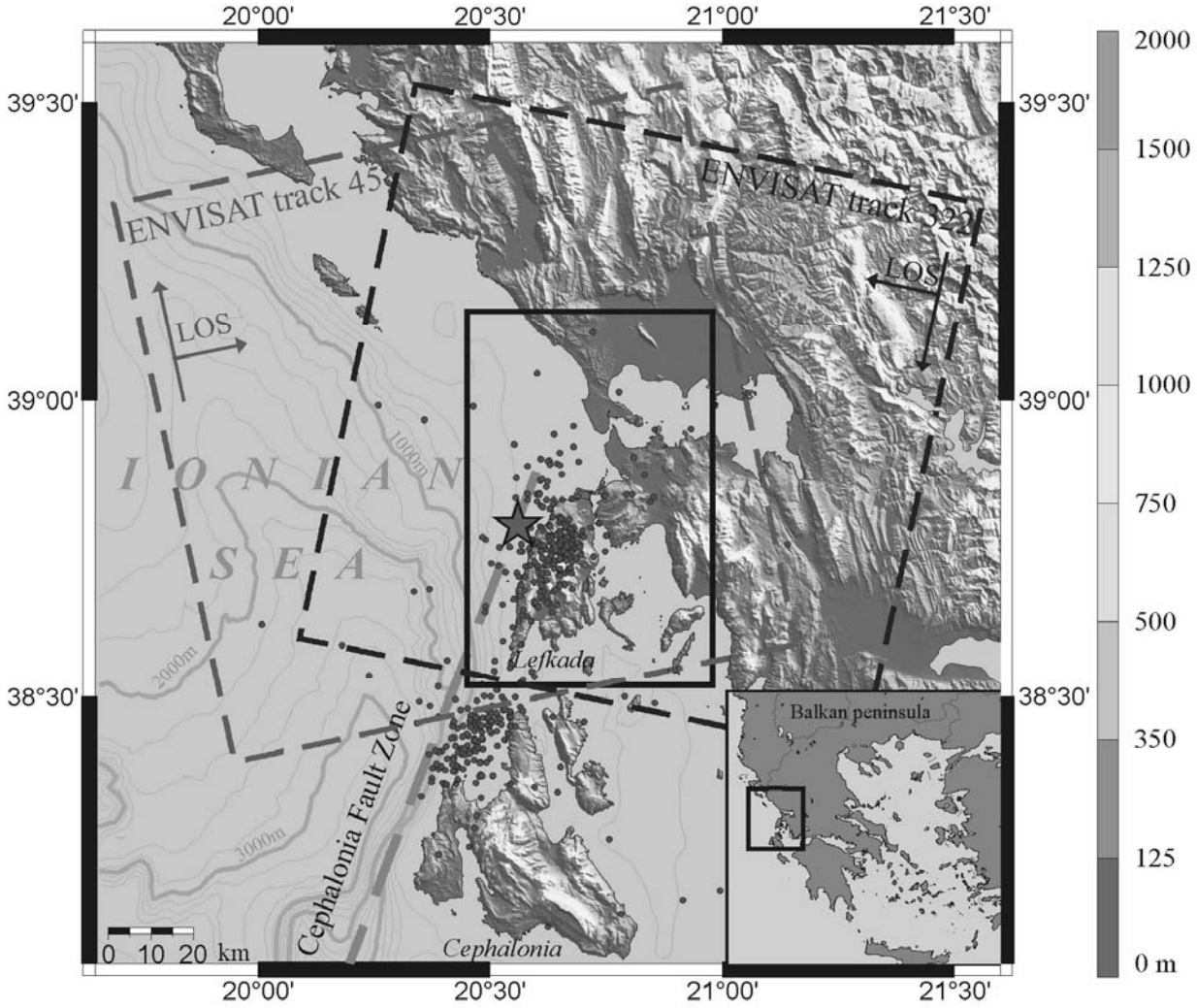

630

631

632 Fig. 5. ENVISAT/ASAR ascending footprint, track 458, frame 774, represented by red
633 dashed rectangle, descending footprint, track 322, frame 2821 – by blue dashed rectangle.
634 Location of 14th August 2003 earthquake from NOA is shown with red star and aftershock
635 sequence by PSL with red dots. The long red arrow represents the satellite flight direction and
636 short arrow is the satellite looking direction (LOS); black rectangle – the area of investigation
637 presented in the next figures; orange dashed line – generalized view of Cephalonia Fault
638 Zone; isobaths – generated from ETOPO1 (Amante and Eakins, 2009); topography – SRTM
639 v4.

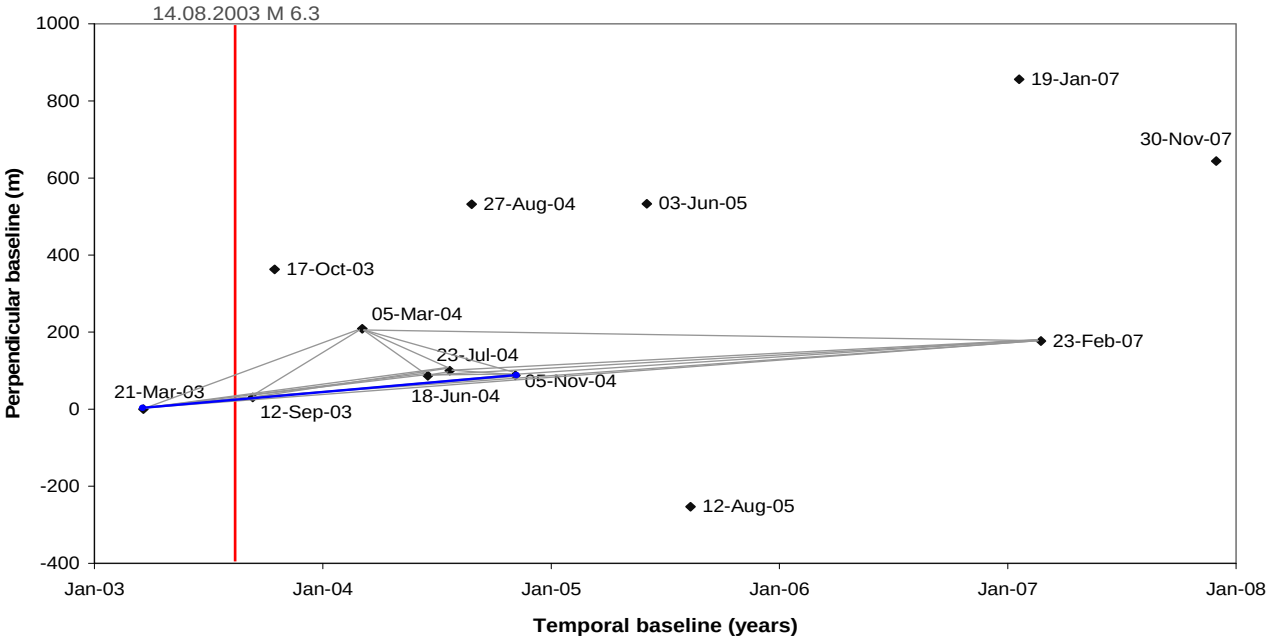

Fig. 6. Available ascending scenes covering the Lefkada Island: with the red line – time of the 14th August 2003 earthquake, with grey lines – the generated interferograms, with blue line – couple with the best quality (*ifg*5: 21.03.2003 – 05.11.2004).

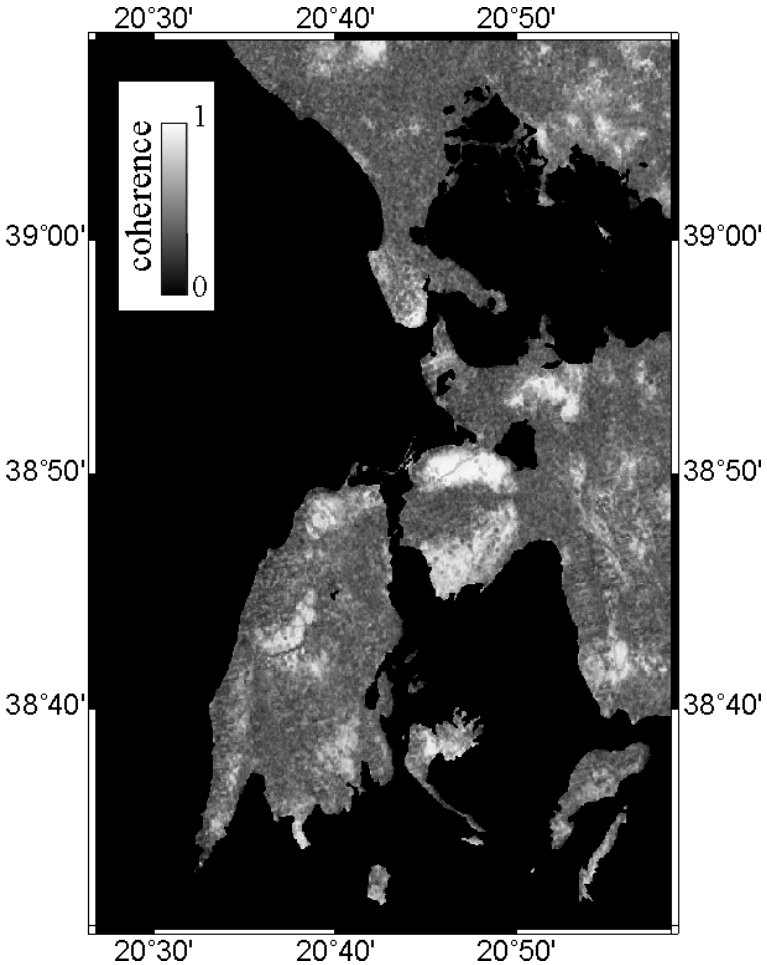

Fig. 7. Coherence map generated from 21 ascending interferograms, showing the mean level of coherence on the territory of the island. The parts which return better signals are in the central and northern part of the area as well as in the closest mainland.

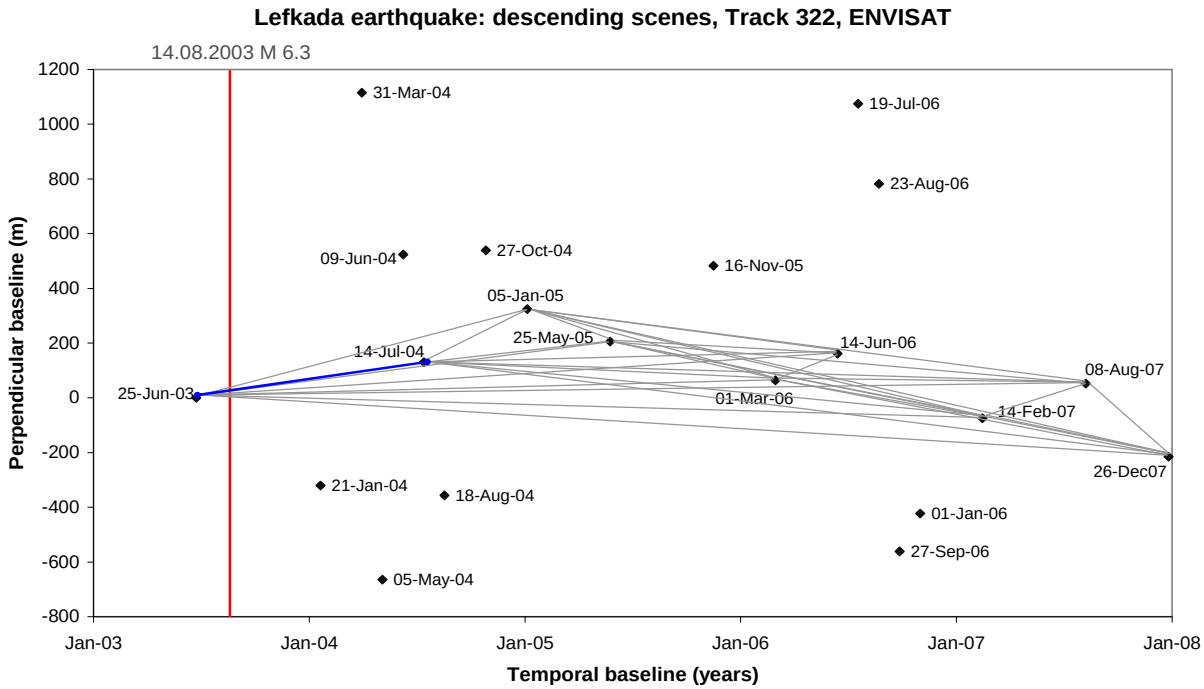

649
650
651 Fig. 8. Available descending scenes covering the Lefkada Island: with the red line – time of
652 the 14th August 2003 earthquake, with grey lines – the generated interferograms, with blue
653 line – couple with the best quality (*ifg*22: 25.06.2003 – 14.07.2004).

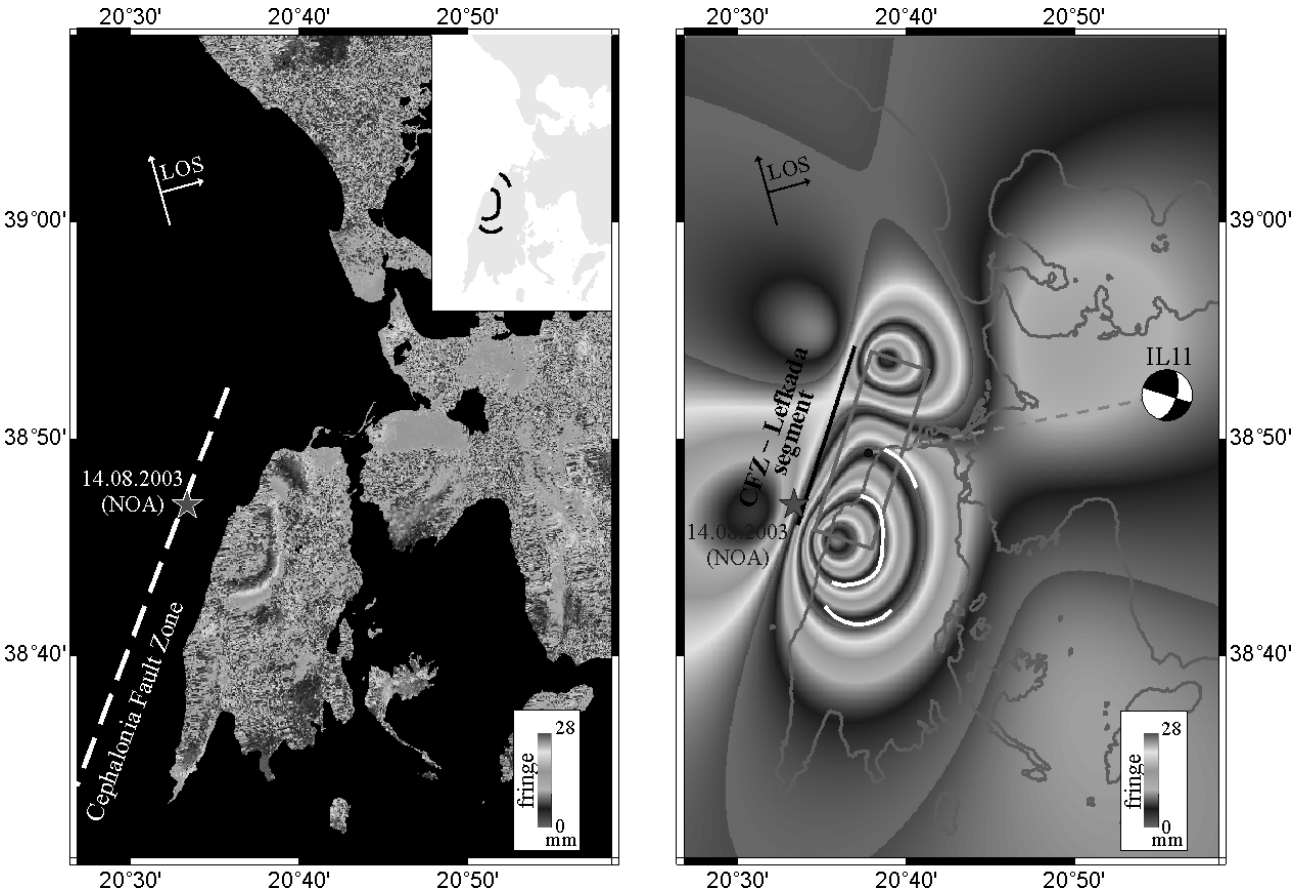

Fig. 9. SAR interferometry results for the Lefkada earthquake. Left: Differential ascending interferogram – *ifg*5 (BL 88m). The star shows the main shock according to NOA; the arrows – direction of ascending flight and side of looking of the satellite. An approximation of the Cephalonia Fault Zone is presented by white dashed line. Inset: The observed fringes. Right: Synthetic ascending interferogram obtained from inversion of the received observed fringes (left). The rectangle represents the approximate model of the fault segment.

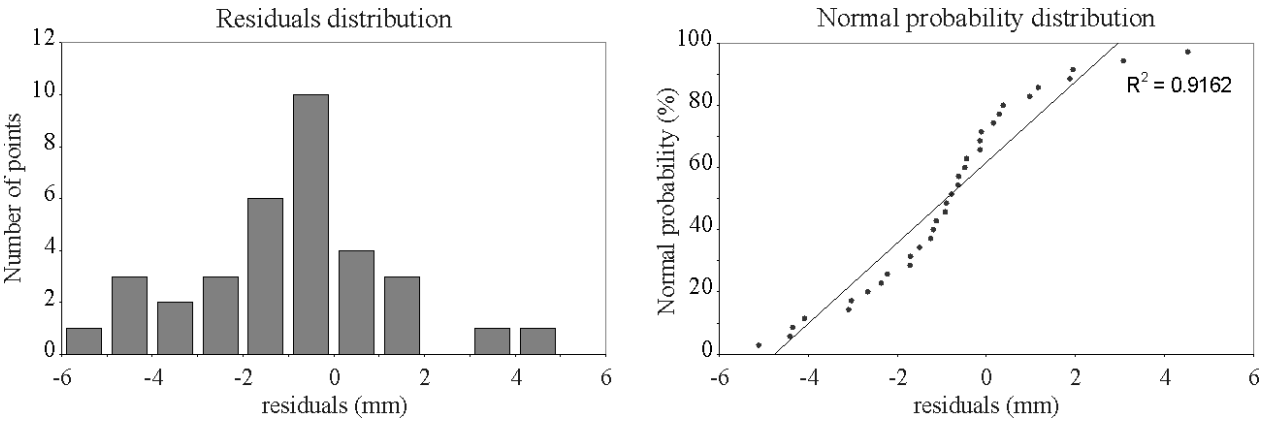

Fig. 10. Left: Residual distribution for the 34 points chosen from the observed fringes. Right: Normal probability plot for the same residual values.

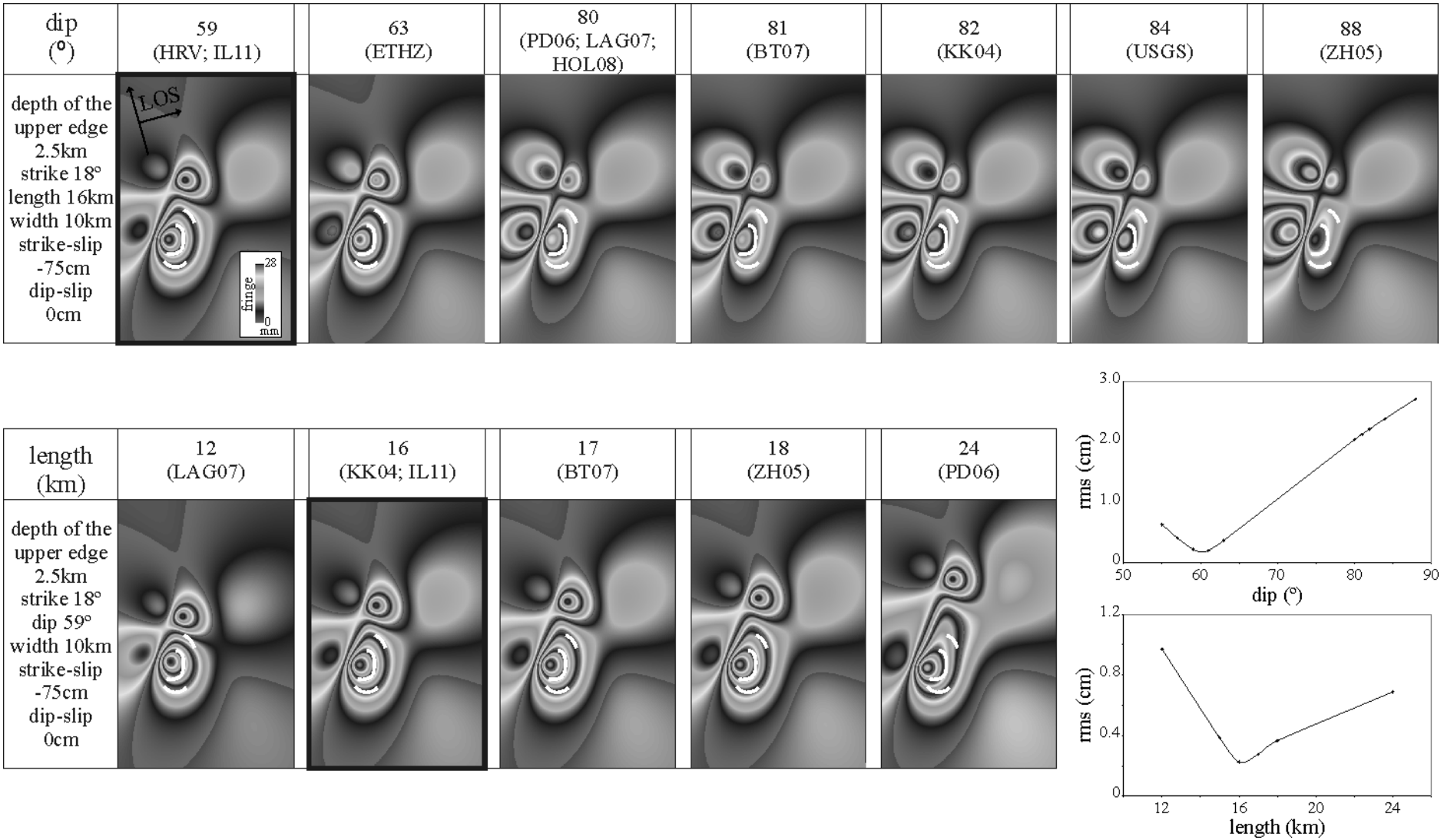

Fig.11. Dip and length confidence study by comparison with the values proposed by previous studies. The notations are the same as for Table 2 and Table 3. To the right: rms misfits plot for the dip and the length respectively, inverted by the InSAR data. All other parameters are fixed (see the left of the figure)

669

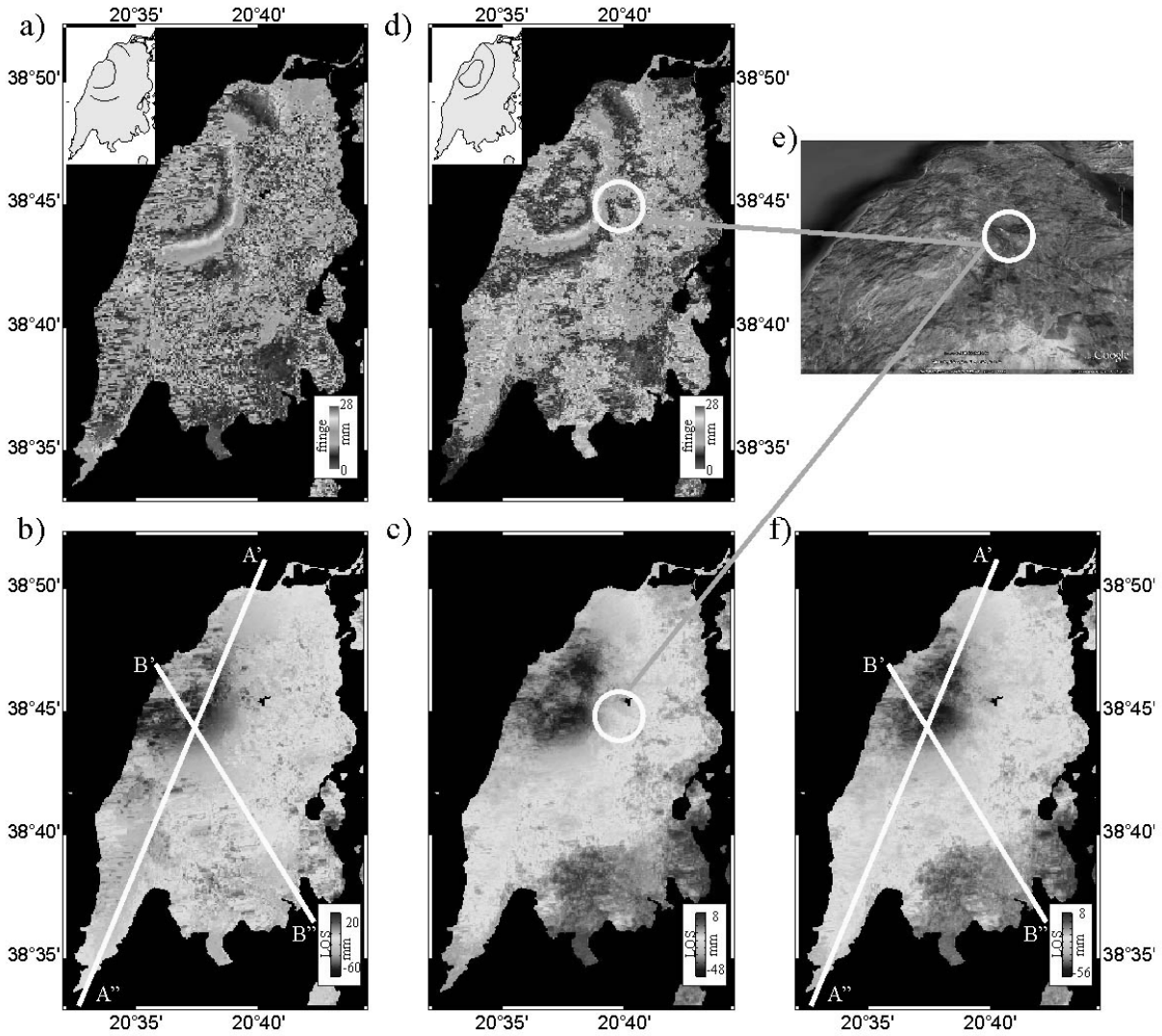

670
671

672 Fig. 12. Stacking of ascending interferograms. (a) The ascending interferogram with the best
673 quality (*ifg*5). (b) The same but unwrapped. (c) Average of the six ascending co-seismic
674 unwrapped interferograms. (d) Re-wrapped stacked interferogram and draped (e) over the
675 *Google Earth* topography of the island. (f) Stacking of five unwrapped interferograms
676 (without *ifg*4).

677

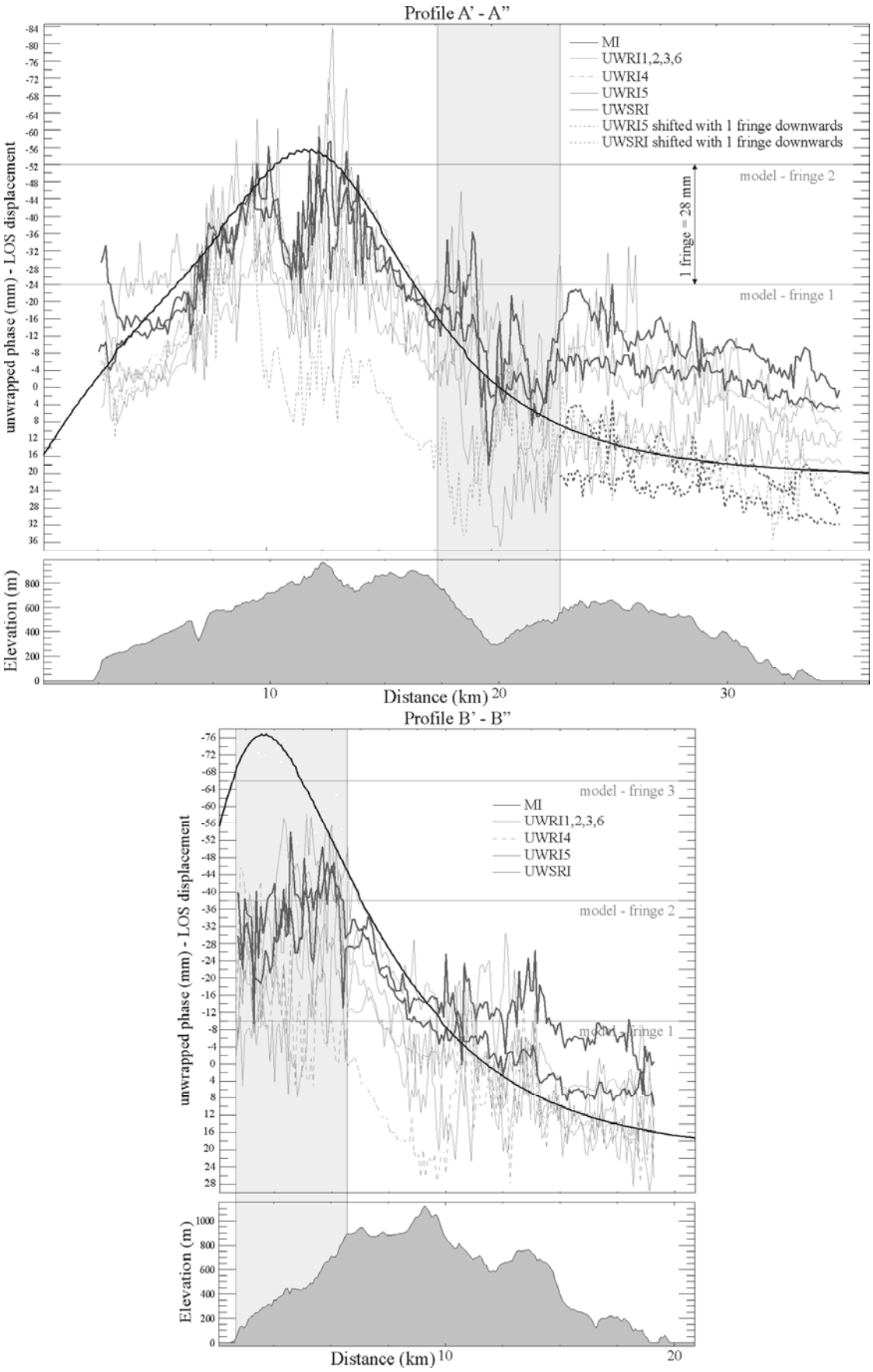

Fig. 13. Unwrapped phases over the profiles A' – A" (up) and B' – B" (down) (see Fig. 12).

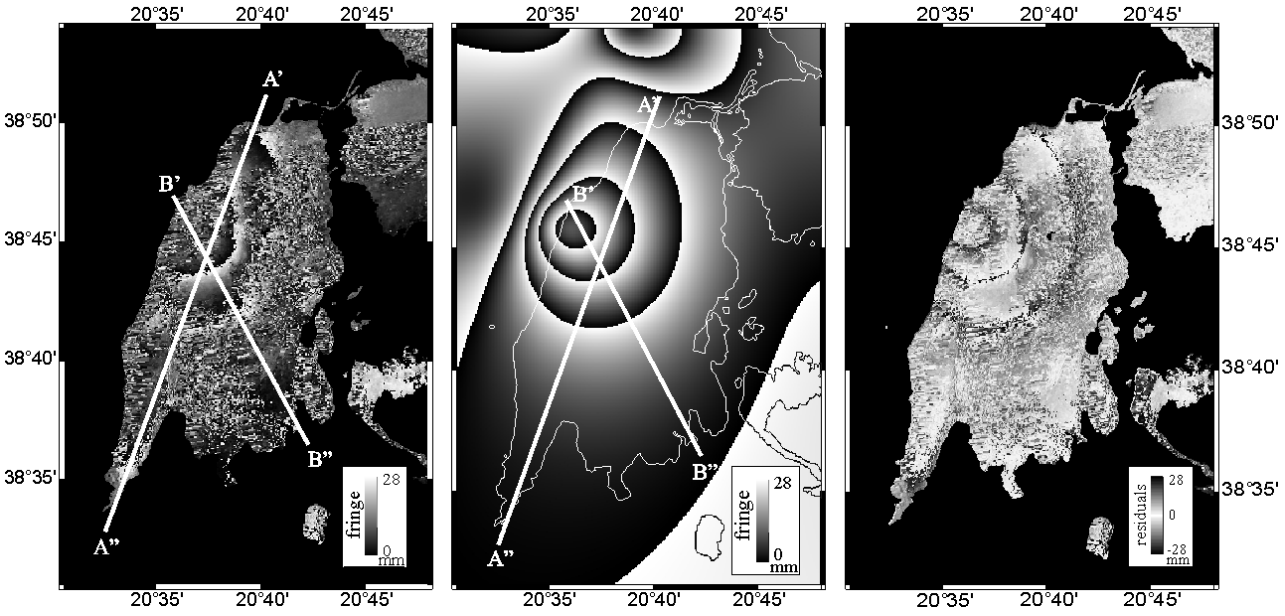

681

682

683 Fig. 14. Residual interferometric pattern (right) compared to the real (left) and synthetic
684 (centre) ascending interferograms

685

686

687

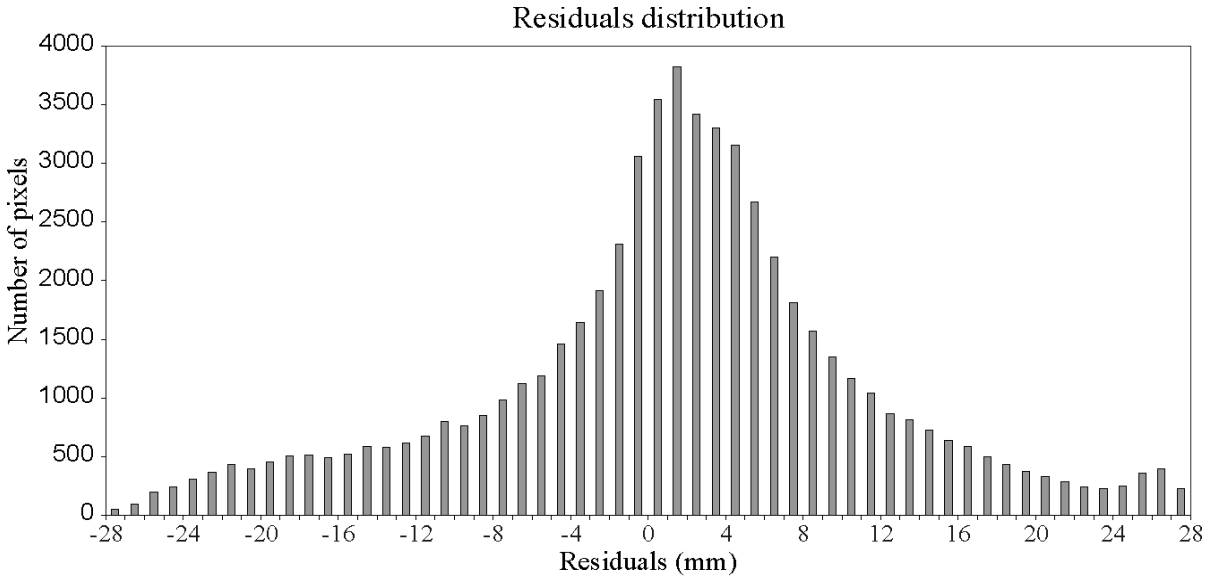

688

689 Fig. 15. Pixel residuals distribution

690

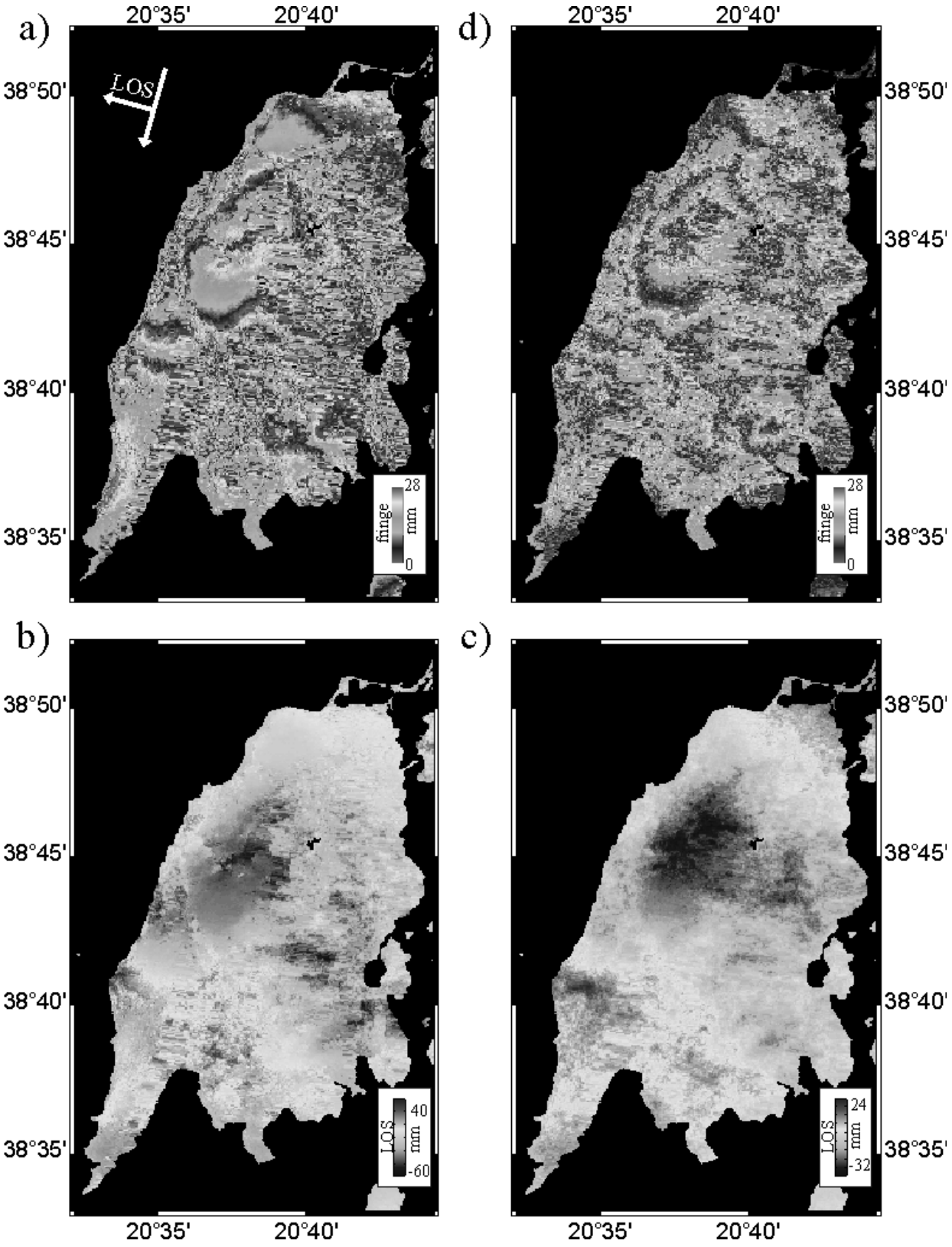

Fig. 16. Stacking of the descending interferograms. (a) The descending interferogram with the best quality (*ifg*22). (b) The same but unwrapped. (c) Average of the eight descending co-seismic unwrapped interferograms. (d) Re-wrapped stacked descending interferogram.

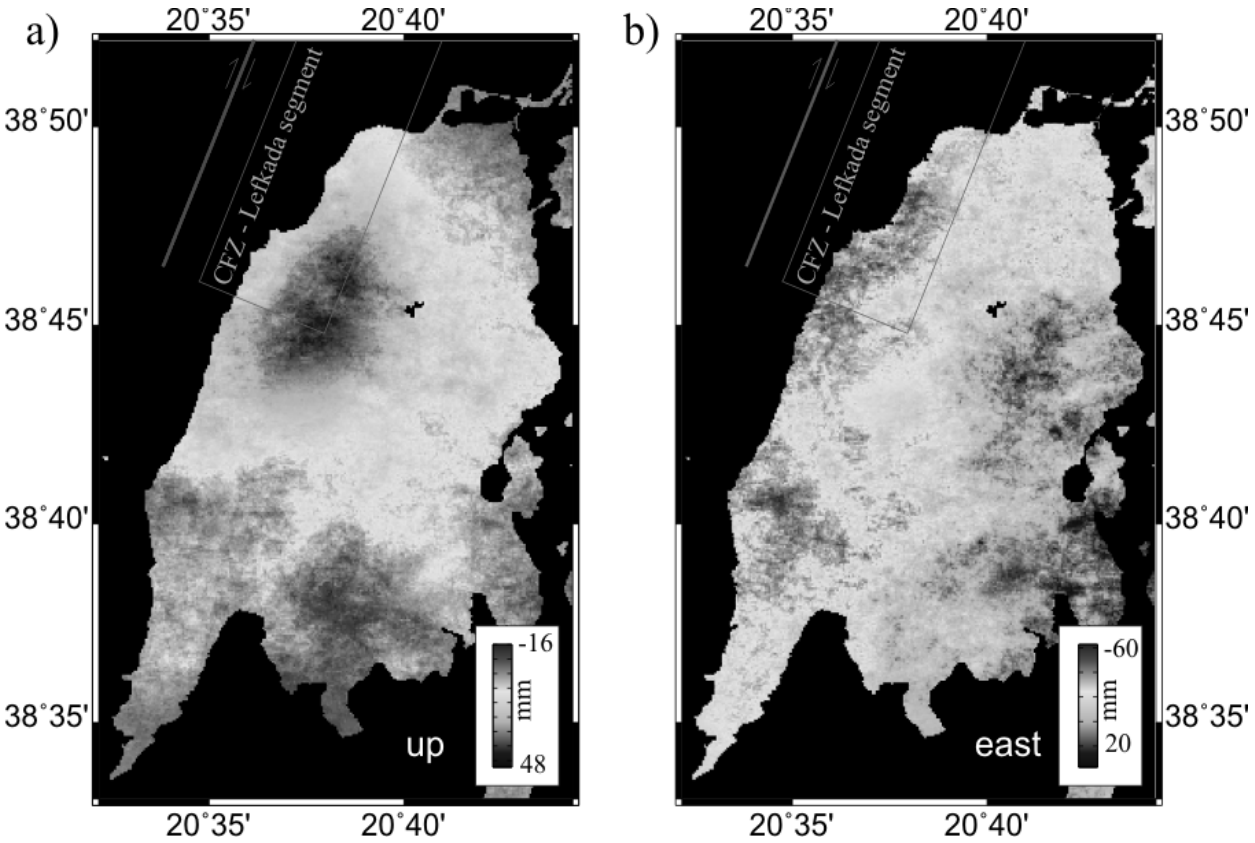

Fig. 17. Theoretical displacements in Up and East directions.

699 **TABLES**
700
701

Date (Y.M.D)	lat (°)	long (°)	M	depth (km)	Io	strike (°)	dip (°)	rake (°)	Mo (* 10^{18} Nm)	length (km)	slip (cm)	Ref.*
1612.05.26	38.8	20.6	6.6		VIII							2 in 1
1613.10.12	38.8	20.8	6.4		VIII							2 in 1
1625.06.28	38.8	20.7	6.6		IX							2 in 1
1630.07.02	38.8	20.8	6.7		IX							4 in 3
1704.11.22	38.8	20.7	6.3		IX							2 in 1
1722.06.05	38.6	20.7	6.4		VIII							2 in 1
1723.02.22	38.6	20.7	6.7		IX							2 in 1
1769.10.12	38.8	20.6	6.7		IX							2 in 1
1783.03.23	38.7	20.61	6.7		X							2 in 1
1815.03.17	38.8	20.7	6.3		VIII							2 in 1
1820.02.21	38.8	20.6	6.4		IX							2 in 1
1825.01.19	38.7	20.6	6.5		X							2 in 1
1869.12.28	38.80	20.65	6.4	3-15	X	1	60	165		26	35	4 in 5
1914.11.27	38.65	20.62	6.3	3-15	IX	16	60	165		23	29	6 in 5
1948.04.22	38.68	20.57	6.5	3-15	IX	1	60	165		30	42	4 in 5
1948.06.30	38.80	20.60	6.4	3-15	IX	1	60	165		26	35	4 in 5
1973.11.04	38.89	20.44	5.8	23	VII+	324	50	81	0.61			8 in 7
1994.02.25	38.76	20.54	5.5	9		22	58	168	0.215			7

702
703 **Table 1.** Historical and instrumental seismicity review. References: 1 – Papathanassiou et al.
704 (2005); 2 – Papazachos et al. (2000); 3 – Fokaefs and Papadopoulos (2004); 4 – Papazachos
705 and Papazachou (1997); 5 – Papadimitriou (2002); 6 – Papazachos et al. (1998); 7 – Louvari
706 et al. (1999); 8 – Baker et al. (1997). The intensity values are according to Papathanassiou et
707 al. (2005) except the event of 1630, whose value is taken from Fokaefs and Papadopoulos
708 (2004).

Ref.*		lat (°)	long (°)	Mw	depth (km)	strike (°)	dip (°)	rake (°)	length (km)	width (km)	Mo (* 10^{18} Nm)	Slip (cm)
HRV		38.70	20.67	6.2	15	18	59	-174	-	-	2.98	-
USGS		39.16	20.60	6.1	21	13	84	172	-	-	2.0	-
MN		38.88	20.62	6.2	24	196	85	-166	-	-	2.6	-
ETHZ		39.24	20.49	6.32	31	97	63	-30	-	-	3.72	-
NOA		38.79	20.56	6.4	12	-	-	-	-	-	-	-
PSL		38.83	20.62	ML 5.85	15.5	-	-	-	-	-	-	-
AUT		38.74	20.54	6.3	11	-	-	-	-	-	-	-
ZH05:	ms	38.84	20.60									
ZH05_1	s1	38.78	20.57	5.7	13	17	88	-177	18	9	0.47	-
ZH05_2	s2	38.46	20.43	5.8	13	24	74	164	-	-	0.49	-
BT07:	av			6.2	13	16	72	178	23	-	2.23	42
BT07_1	s1	38.78	20.57	6.0	11	12	81	174	17	10	1.3	34
BT07_2	s2	38.50	20.44	5.8	15	20	63	-179	13	10	0.65	23
PD06		38.86	20.56	6.3	9	15	80	170	24	2-12	2.9	40

Table 2. Published source parameters for the 2003 August 14 Lefkada earthquake (compared also in Fig. 4). ms – main shock, s1 – sub-event 1, s2 – sub-event 2, av – averaged.
* HRV – CMT Harvard ; USGS – U.S. Geological Survey; MN – MedNet (Mediterranean Very Broadband Seismographic Network – INGV) in Zahradník et al. (2005); ETHZ – Swiss Federal Institute of Technology Zurich; NOA – National Observatory of Athens, Institute of Geodynamics; PSL – Patras Seismological Laboratory; AUT – Aristotle University of Thessaloniki; ZH05_1 and ZH05_2 – 1 and 2 sub-events in Zahradník et al. (2005); BT07_1 and BT07_2 – 1 and 2 sub-events in Benetatos et al. (2007); PD06 - Papadimitriou et al. (2006).

Ref.	lat (°)	long (°)	Mw	depth (km)	strike (°)	dip (°)	rake (°)	L (km)	W (km)	Mo (* 10^{18} Nm)	slip (cm)
LOU99	-	-	-	-	14	65	167	40	15	-	-
PD02 ¤	38.71	20.58	-	15	11	60	+165	-	-	-	-
KK04	-	-	-	3-12	-	-	-	16	-	-	~60
LAG07	-	-	-	13	15	80	174*	12	11	-	-45
HOL08	38.60	20.50	6.3*	7	15	80	180*	60	10	2.97	16.5
model in this study (IL16)	**38.83 #**	**20.64#**	**6.3**	**6.8 #**	**18**	**59**	**180**	**16**	**10**	**3.60**	**75**
Uncertainties of our model	**0.01**	**0.01**		**1.**	**3.**	**5.**	**8.**	**2.**	**2.**		**15**

Table 3. Other fault plane solutions for Lefkada Segment of Cephalonia Fault Zone (compared also in Fig. 4). The coordinates are for the centre of the fault. * estimated here; ¤ - after Papazachos et al. (1998); # - centre of the fault; L – length; W –width; LOU99 – Louvari et al. (1999); PD02 – Papadimitriou (2002); KK04 – Karakostas et al. (2004); LAG07 – Lagios et al. (2007); HOL08 – Hollenstein et al. (2008).

728

Ni	Pass	Date 1	Date 2	Days	$B_{\perp}$ (mm)	h_a (m)	e^h_{max}(mm)
ifg 1	A	21.03.2003	12.09.2003	174	-35	268	2
ifg 2	A	21.03.2003	05.03.2004	349	-209	45	10
ifg 3	A	21.03.2003	18.06.2004	453	-87	108	4
ifg 4	A	21.03.2003	23.07.2004	489	-104	90	5
***ifg* 5**	**A**	**21.03.2003**	**05.11.2004**	**592**	**-88**	**107**	**4**
ifg 6	A	21.03.2003	23.02.2007	1432	-177	53	8
ifg 7	A	12.09.2003	05.03.2004	175	-179	52	9
ifg 8	A	12.09.2003	18.06.2004	280	-56	167	3
ifg 9	A	12.09.2003	23.07.2004	315	-70	134	3
ifg 10	A	12.09.2003	05.11.2004	419	-57	165	3
ifg 11	A	12.09.2003	23.02.2007	1258	-146	64	7
ifg 12	A	05.03.2004	18.06.2004	104	122	77	6
ifg 13	A	05.03.2004	23.07.2004	140	109	86	5
ifg 14	A	05.03.2004	05.11.2004	243	121	77	6
ifg 15	A	05.03.2004	23.02.2007	1082	32	293	2
ifg 16	A	18.06.2004	23.07.2004	35	-18	521	1
ifg 17	A	18.06.2004	05.11.2004	139	-6	1563	0
ifg 18	A	18.06.2004	23.02.2007	978	-92	102	4
ifg 19	A	23.07.2004	05.11.2004	104	18	521	1
ifg 20	A	23.07.2004	23.02.2007	943	-77	122	4
ifg 21	A	05.11.2004	23.02.2007	839	-92	102	4
***ifg* 22**	**D**	**25.06.2003**	**14.07.2004**	**385**	**-118**	**79**	**6**
ifg 23	D	25.06.2003	05.01.2005	560	-300	31	14
ifg 24	D	25.06.2003	25.05.2005	700	-201	47	9
ifg 25	D	25.06.2003	01.03.2006	980	-48	195	2
ifg 26	D	25.06.2003	14.06.2006	1085	-154	61	7
ifg 27	D	25.06.2003	14.02.2007	1330	79	119	4
ifg 28	D	25.06.2003	08.08.2007	1505	-45	208	2
ifg 29	D	25.06.2003	26.12.2007	1645	212	44	10

729

730 **Table 4.** Details for the ascending (A) and descending (D) interferograms processed for this
731 study, where Ni – number of interferogram, B – perpendicular baseline (m), Days – offset
732 between acquisition of the two images; h_a – altitude of ambiguity; e^h_{max} – maximum error due
733 to the topography. The bold lines show the best ascending (A) and descending (D)
734 interferograms.

Scene date	Pass	Mean temperature (°C)	Mean pressure at sea level (hPa)	Mean humidity (%)	Wind (m/s)	Cloudiness (%)	Cloud base altitude (m)	Precipitation
21.03.2003	**A**	**+10.6**	**1016**	**74**	**4**	**20**	**1750-3000**	**None**
12.09.2003	A	+22.6	1013	75	5	40	800	None
05.03.2004	A	+ 9.4	1014	54	6	80	800-2250	None
18.06.2004	A	+22.8	1004	72	3	50	800	Rain or Drizzle
23.07.2004	A	+27.3	1014	71	3	10	3000	None
05.11.2004	**A**	**+18.1**	**1018**	**54**	**8**	**10**	**800-2250**	**None**
23.02.2007	A	+11.8	1011	90	3	30	450-2250	None
25.06.2003	**D**	**+26.6**	**1014**	**78**	**3**	**20**	**1750-3000**	**None**
14.07.2004	**D**	**+23.3**	**1011**	**57**	**6**	**20**	**800**	**None**
05.01.2005	D	+7.4	1028	75	1	30	3000	None
25.05.2005	D	+20.4	1014	85	1	30	800	None
01.03.2006	D	+11.6	1013	75	0	70	800	Mist
14.06.2006	D	+19.3	1019	80	5	20	800	None
14.02.2007	D	+12.1	1009	72	6	40	800	27 mm
08.08.2007	D	+24.3	1013	82	3	20	450-3000	None
26.12.2007	D	+10.0	1025	94	3	50	250-800	15 mm, Fog, Rain and Drizzle

Table 5. ENVISAT images used in the research and the weather conditions during their acquisitions according to the weather archives for Aktion Airport (38°37'N 20°46'E) (http://meteo.infospace.ru; http://www.tutiempo.net). The bold lines correspond to the dates of acquisition of the images used for the best ascending and descending interferograms.

Source of empirical relationship	L (Surface rupture length) - km	W (Down-dip rupture width) - km	U (Average displacement) - cm
Konstantinou *et al.* (2005)	$\log L = -1.49 + 0.47 M_w$ L = 29	$\log W = -1.07 + 0.34 M_w$ W = 11	
Papazachos & Papazachou (1997)	$\log L = -1.85 + 0.51 M_w$ L = 23	$\log W = -0.13 + 0.19 M_w$ W = 12	$\log u = -3.71 + 0.82 M_w$ u = 24
Well & Coppersmith (1994)	$\log L = -3.55 + 0.74 M_w$ L = 13	$\log W = -0.76 + 0.27 M_w$ W = 9	
this study	**L = 16**	**W = 10**	**u = 75**

Table 6. Comparison between Length-Magnitude empirical relations and calculated fault dimensions

Long (°)	Lat (°)	UTM_E (km)	UTM_N (km)	LoS observed (mm)	LoS modelled (mm)
20.5765	38.6244	463.16	4275.20	24.4	7.2
20.5793	38.6332	463.41	4276.17	24.4	8.4
20.5853	38.6428	463.93	4277.24	24.4	10.2
20.5874	38.6558	464.11	4278.67	24.4	12.8
20.5884	38.6646	464.20	4279.64	24.4	14.9
20.5891	38.6709	464.26	4280.34	24.4	16.7
20.5909	38.6794	464.42	4281.29	24.4	19.6
20.5916	38.6844	464.48	4281.83	24.4	21.4
20.5926	38.6929	464.57	4282.78	24.4	24.9
20.5975	38.6984	465.00	4283.39	24.4	27.8
20.6084	38.7001	465.96	4283.57	24.4	28.9
20.6236	38.7042	467.28	4284.03	24.4	29.9
20.6335	38.7097	468.15	4284.64	24.4	30.8
20.6415	38.7166	468.85	4285.40	24.4	31.8
20.6493	38.7246	469.53	4286.28	24.4	32.5
20.6524	38.7345	469.81	4287.38	24.4	34.5
20.6588	38.7433	470.36	4288.35	24.4	33.8
20.6602	38.7524	470.49	4289.35	24.4	34.5
20.6630	38.7601	470.73	4290.21	24.4	33.6
20.6637	38.7692	470.79	4291.21	24.4	32.9
20.6608	38.7758	470.54	4291.94	24.4	33.5
20.6584	38.7857	470.33	4293.04	24.4	32.4
20.6516	38.7934	469.74	4293.89	24.4	32.9
20.5889	38.7416	464.25	4288.16	52.4	53.1
20.5971	38.7367	464.96	4287.61	52.4	50.9
20.6084	38.7347	465.95	4287.40	52.4	49.3
20.6193	38.7356	466.91	4287.50	52.4	47.6
20.6316	38.7370	467.99	4287.65	52.4	44.1
20.6351	38.7419	468.29	4288.20	52.4	44.7
20.6394	38.7469	468.66	4288.74	52.4	44.2
20.6397	38.7521	468.69	4289.32	52.4	45.3
20.6383	38.7593	468.57	4290.11	52.4	47.2
20.6354	38.7686	468.32	4291.15	52.4	48.8
20.6294	38.7799	467.79	4292.39	52.4	49.7

Table 7. The 34 picked values on the two visible ascending fringes in the best ascending interferogram. The origin for the LoS was estimated during the joint inversion process. The coordinates are also given in UTM 34.

Long (°)	Lat (°)	UTM_E (km)	UTM_N (km)	LoS observed (mm)	LoS modelled (mm)
20.6485	38.7945	469.46	4294.01	54.4	41.8
20.6358	38.7901	468.35	4293.52	54.4	51.4
20.6227	38.7804	467.21	4292.45	54.4	65.3
20.6136	38.7738	466.40	4291.72	54.4	71.7
20.6072	38.7625	465.85	4290.47	54.4	74.9
20.5998	38.7523	465.20	4289.35	54.4	70.0
20.5978	38.7375	465.02	4287.70	54.4	59.6
20.6003	38.7262	465.24	4286.46	54.4	52.4
20.6042	38.7144	465.58	4285.15	54.4	45.4
20.6151	38.7078	466.54	4284.42	54.4	43.9
20.6268	38.7084	467.56	4284.49	54.4	46.2
20.6366	38.7119	468.42	4284.88	54.4	49.1
20.6458	38.7205	469.22	4285.83	54.4	54.1
20.6574	38.7331	470.24	4287.23	54.4	58.2
20.6630	38.7453	470.73	4288.56	54.4	59.6
20.6665	38.7587	471.04	4290.05	54.4	57.8
20.6686	38.7689	471.22	4291.18	54.4	53.5
20.6651	38.7813	470.91	4292.55	54.4	47.5
20.6615	38.7907	470.60	4293.58	54.4	40.7
20.6545	38.7945	469.98	4294.01	54.4	39.5

Table 8. The 20 picked values on the visible fringe in the best descending interferogram. The origin for the LoS was estimated during the joint inversion process. The coordinates are also given in UTM 34.

Ref.	lat (°)	long (°)	depth (km)	strike (°)	dip (°)	rake (°)	L (km)	W (km)	Mo (* 10^{18} Nm)	slip (cm)
model in this study (IL16)	38.83	20.64	6.8	18	59	180	16	10	3.60	75
alternative model using the combination of ascending and descending interferograms	38.83	20.63	8.8	18	59	180	16	10	3.50	73

Table 9. Comparison of the fault models from ascending interferograms only (IL16, see Table 3) and from a combination ascending of descending interferograms. The coordinates are for the centre of the fault.

APPENDIX A. ENVISAT ascending co-seismic interferograms

Wrapped (top) and unwrapped (bottom) ascending co-seismic interferograms (numbers correspond to the interferogram number in Table 4)

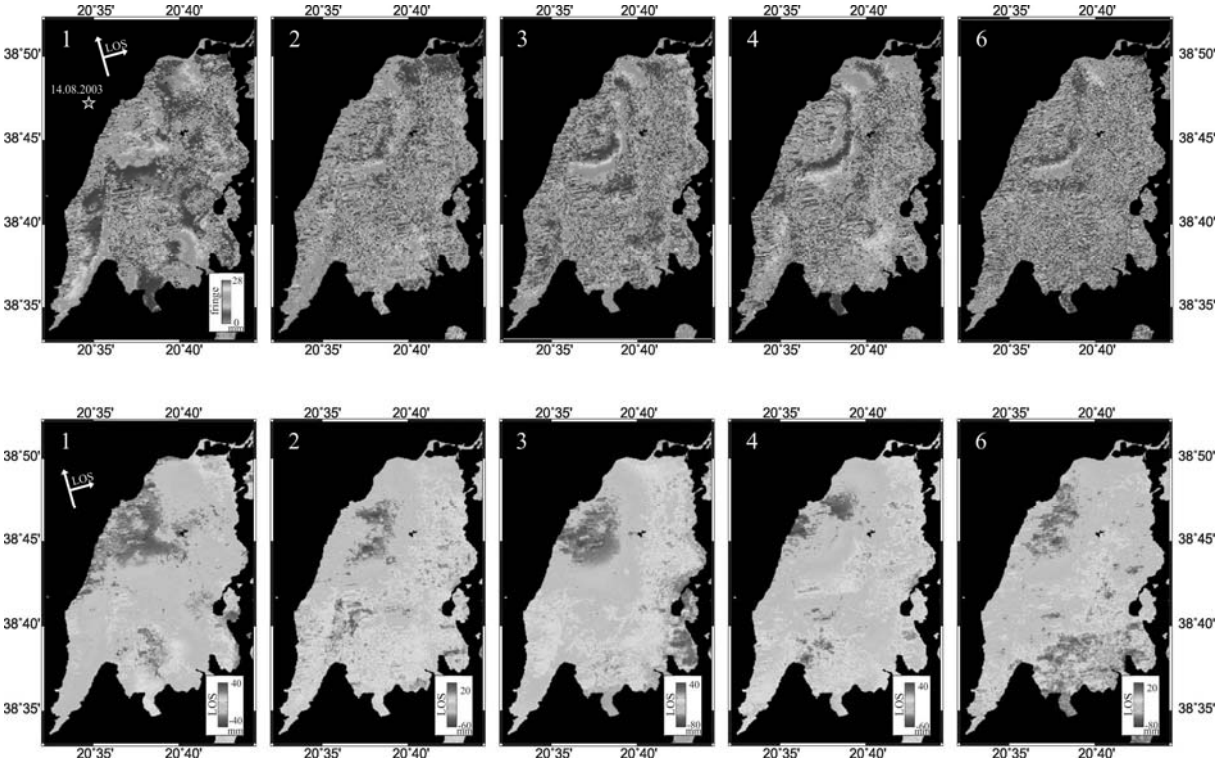

APPENDIX B. ENVISAT ascending post-seismic interferograms

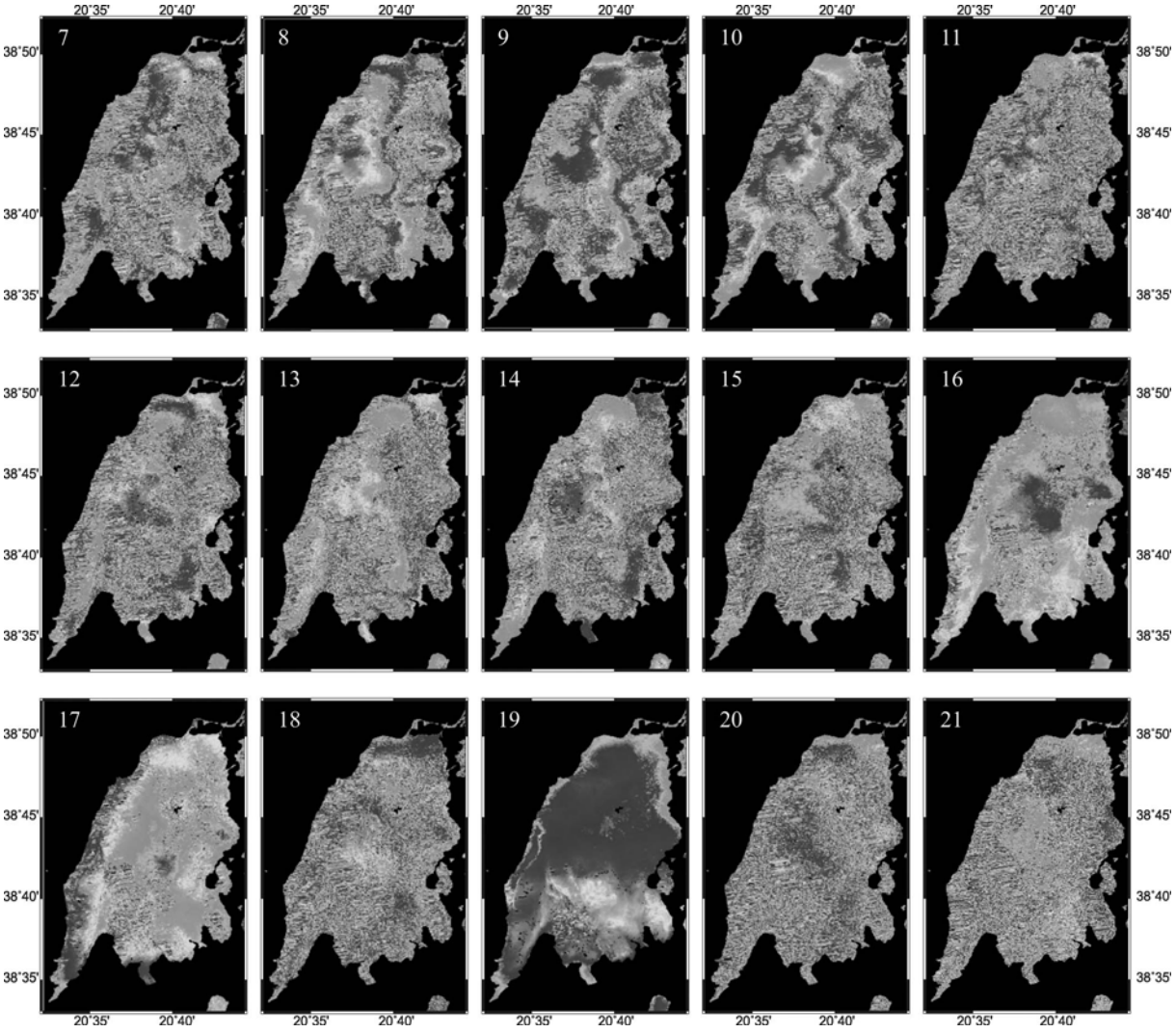

APPENDIX C. ENVISAT descending co-seismic interferograms

Wrapped (top) and unwrapped (bottom) descending co-seismic interferograms (numbers correspond to the interferogram number in Table 4)